

Article

**Chronoamperometric Study of Conformational Relaxation in PPy(DBS)**

B. Jason West, Toribio F. Otero, Benjamin Shapiro, and Elisabeth Smela

*J. Phys. Chem. B*, **2009**, 113 (5), 1277-1293 • DOI: 10.1021/jp8058245 • Publication Date (Web): 14 January 2009

Downloaded from <http://pubs.acs.org> on February 23, 2009

**More About This Article**

---

Additional resources and features associated with this article are available within the HTML version:

- Supporting Information
- Access to high resolution figures
- Links to articles and content related to this article
- Copyright permission to reproduce figures and/or text from this article

[View the Full Text HTML](#)

# Chronoamperometric Study of Conformational Relaxation in PPy(DBS)

B. Jason West,<sup>†</sup> Toribio F. Otero,<sup>||</sup> Benjamin Shapiro,<sup>‡</sup> and Elisabeth Smela<sup>\*,§</sup>

Department of Materials Science and Engineering, Department of Aerospace Engineering, and Department of Mechanical Engineering, University of Maryland, College Park, Maryland 20742, and Dpto. De Arquitectura y Tecnologías de la Edificación, Universidad Politécnica de Cartagena, ETSII C/Carlos III, s/n, 30203 Cartagena, Spain

Received: July 2, 2008; Revised Manuscript Received: November 5, 2008

In conjugated polymer devices that switch from one oxidation level to another, such as artificial muscles, it is important to understand memory effects that stem from conformational relaxation movements of the polymer chains. Chronoamperometry during electrochemical switching of polypyrrole doped with dodecylbenzenesulfonate, PPy(DBS), is used to gain insight into the conformational relaxation processes in cation-transporting materials. During oxidation, the current decays exponentially with a time constant that decreases with the anodic voltage. During reduction, there is again an exponentially decaying current with a time constant that decreases with the cathodic voltage, but superimposed on that is a small current peak that increases in size with the voltage. This peak accounts for a maximum of ~20% of the total reduction charge, which is approximately the same amount of charge that is in the most cathodic pair of peaks in the cyclic voltammogram. The position of this peak depends logarithmically on the applied cathodic potential (shifting to shorter times with larger  $E_{ca}$ ) as well as on the anodic potential that was applied just prior to the reduction step (shifting to longer times with  $E_{an}$ ). Furthermore, the shoulder position depends logarithmically on the time that the prior anodic voltage was held (shifting to longer times with  $t_{wait}$ ). These results are consistent with the electrochemically stimulated conformational relaxation (ESCR) model.

## 1. Introduction

**1.1. Background.** The electrochemical switching of conjugated polymers between the oxidized and reduced states is accompanied by changes in volume, color, conductivity, and other properties. These transformations are employed in actuators (artificial muscles) and a range of other devices, from electrochromic displays to energy storage devices (batteries, supercapacitors).

During oxidation, electrons are removed from the conjugated polymer, and during reduction they are returned. Overall charge neutrality in the material during reduction and oxidation (redox) is maintained by the ingress and egress of ions, supplied by an electrolyte with which the polymer is in contact. *Without this ion transport, the electrochemical reaction cannot proceed.* The ions are solvated, with the size of the solvation shell depending on the ion. It is thus of importance to understand how the physical processes occurring during redox control the rate of ion transport, since this determines how fast the artificial muscles can move, how fast the displays can be refreshed, or how fast the batteries can supply charge.

Conjugated polymers are polymerized in the oxidized state, with the positive charge on the polymer chains compensated by anions. Approximately one anion is incorporated into the polymer for every three pyrrole units. The nature of these “dopant” anions strongly affects the material properties and the switching behavior. For actuators, one of the most significant

properties of the dopant anion is its size. As a rule of thumb, although this not always the case,<sup>1</sup> if the anions are small (such as  $\text{ClO}_4$  or  $\text{PF}_6$ ), then upon reduction these anions exit the polymer, and during oxidation small anions from the electrolyte re-enter.<sup>2,3</sup> However, if the anions are sufficiently large (such as dodecylbenzenesulfonate (DBS) or polystyrenesulfonate (PSS)), then they can be trapped in the polymer, particularly in polymers such as polypyrrole (PPy) that are cross-linked. Since the anions cannot exit the material upon reduction, charge neutrality is primarily maintained by the ingress of cations, which exit the material during oxidation.

The magnitude of the volume change (i.e., the engineering strain  $\Delta l/l$ , where  $l$  is the initial length) depends on the effective size of the ion. For example, in aqueous electrolytes  $\text{Li}^+$  has a larger hydration shell (surrounding number of water molecules) than  $\text{K}^+$ , and this leads to greater strain.<sup>4</sup> There can also be independent water movement that causes significant strain: the osmotic effect due to charges inside the material leads to the influx of water.<sup>5</sup> The ingress of ions and water leads to a volume expansion, and their egress to contraction, which is exploited in actuators. The various redox states are illustrated schematically in Figure 1.

**1.2. Conformational Relaxation.** The ingress of ions and water requires the creation of free volume in the material, which takes energy. [The electrical energy supplied during switching is consumed by the electrochemical reaction itself, by the movement of the ions, by conformational movements of the chains, and by Joule heating due to resistances in the system.] This is a key concept. If the polymer is initially in a compact state that the ions cannot enter, then additional energy is required to allow the chains to change conformation and move apart: in this case, the rate-limiting step of the reaction (which controls the oxidation or reduction speed) becomes the conformational

\* Corresponding author: Tel (301) 405-5265; Fax (301) 314-9477; e-mail smela@eng.umd.edu.

<sup>†</sup> Department of Materials Science and Engineering, University of Maryland.

<sup>‡</sup> Department of Aerospace Engineering, University of Maryland.

<sup>§</sup> Department of Mechanical Engineering, University of Maryland.

<sup>||</sup> Universidad Politécnica de Cartagena.

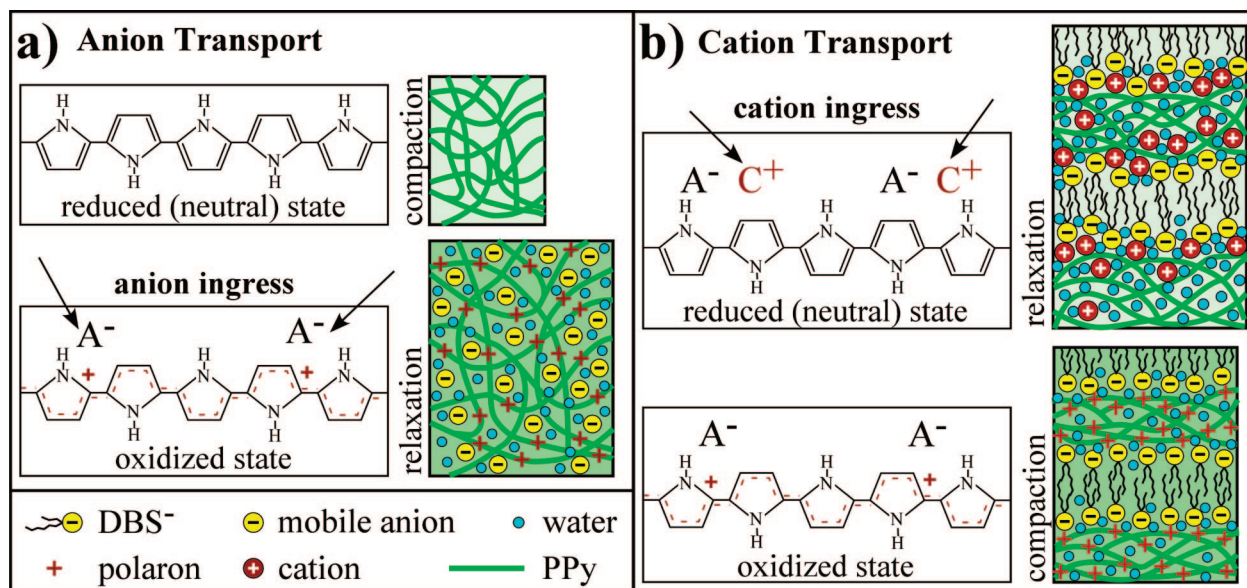


**Figure 1.** Schematic illustration of redox in (a) a general anion-transporting PPy and (b) the cation transporter PPy(DBS), which has a lamellar structure. In (a), hydrated anions enter the polymer during switching to the oxidized state to maintain charge neutrality, which requires PPy chain relaxation. In (b), hydrated cations enter during switching to the reduced state, which also requires relaxation.

relaxation rate. (The matrix can be considered closed when the average distance between neighboring polymeric chain segments is smaller than the size of the charge-compensating solvated ion entering from the solution). The dependence of ion ingress on the degree of compaction of the polymer has been thoroughly studied in anion-transporting materials and has been well described using the electrochemically stimulated conformational relaxation (ESCR) model.<sup>7–9</sup> The ESCR model has been shown to account for the behavior of a wide range of materials under a wide range of experimental conditions.

In chronoamperograms of anion-transporting polymers, conformational relaxation manifests itself as a peak in the anodic (oxidation) current (see Figure 21a in the Discussion section for an example) whose position in time depends on experimental variables such as the applied anodic voltage,<sup>7–9</sup> the cathodic voltage applied preceding the anodic step,<sup>7–12</sup> the time spent at that cathodic voltage,<sup>13–15</sup> the temperature,<sup>7–9,16,17</sup> the solvent,<sup>18</sup> the size of the ion,<sup>6</sup> the type of polymer,<sup>8</sup> the number of cycles performed,<sup>19</sup> and the electrolyte concentration.<sup>9</sup> There is no corresponding cathodic (reduction) peak during anion egress, since the polymer is already in an expanded state and thus has the necessary free volume to allow ion movement.<sup>20</sup>

This coupling of ion ingress, volume change, and energy is the basis for the use of conjugated polymers as artificial muscles. (On the other hand, it can be problematic for electrochromic and energy storage applications that may suffer from volume change.) Controlling the degree of compaction of the matrix is important, since if the polymer could always be kept in a more expanded state, then devices could be switched faster. It is also important to understand conformational relaxation effects since they give the polymer a “memory”: the previous state (oxidized or reduced) of the polymer, and how long it was held there, affect how quickly it responds to a signal to change its oxidation level. Mathematical models that quantify conformational relaxation and relate it to redox speed must therefore be included in control schemes for conjugated polymer devices.

Conformational energy not only is critical in actuation of conjugated polymers but also is the origin of their sensing properties. The link between conformational energy and electrochemical energy allows these materials to be used as load

sensors (and thus to be used in feedback-control systems),<sup>21,22</sup> chemical sensors,<sup>23</sup> and thermal sensors,<sup>23</sup> since mechanical force, chemical reactions, and temperature all affect the conformational energy, which can be measured electrochemically.

To understand these complex interrelationships between ion movements, chain conformations, chemical reactions, and energy (and to develop mathematical models), it is necessary to control the experimental conditions so that the reaction is controlled by a single rate-limiting step (i.e., the slowest step). In this paper, we are concerned with the conformational changes in the polymer, so the experiments were designed to establish a particular state of the polymer matrix prior to electrochemical switching and to keep the other variables constant.

**1.3. Switching of PPy(DBS).** Cation-transporting materials are important in actuators,<sup>24–27</sup> but conformational relaxation in these materials is not yet understood. In this work we examine conformational relaxation effects in PPy doped with DBS, PPy(DBS), which has been used extensively in our microactuators.<sup>2,28–30</sup> We examine the chronoamperograms of PPy(DBS) as a function of oxidation and reduction potentials as well as the time held at an oxidizing potential. It is known that higher cathodic (negative) potentials increase the speed of the reduction reaction<sup>31</sup> by increasing the speed of cation migration into the polymer.<sup>32</sup> On the basis of ESCR, it is expected that higher cathodic potentials will also lead to faster responses by providing greater energy for chain movements. (Energy and voltage are directly related; see eq 2.) Higher anodic potentials, on the other hand, are expected to increase the degree of compaction of the polymer matrix, slowing down subsequent reduction reactions by bringing them under increasing conformational relaxation control. The degree of polymer compaction has already been observed to affect cation mobility in PPy(DBS), with mobility increasing strongly as the polymer takes on an increasingly open state during the reduction process.<sup>31</sup>

The behavior of PPy(DBS) is expected to differ from that of anion-transporting PPy not only because cations enter during reduction, rather than anions entering during oxidation, but also because the DBS that is incorporated during material synthesis is a surfactant that imparts a lamellar morphology to the PPy<sup>33</sup> (Figure 1), which none of the previously examined anion-

transporting polymers have had. Ion transport parallel to the lamellae is much faster than perpendicular to them, through the PPy chains,<sup>4</sup> and out-of-plane expansion<sup>34,35</sup> is much greater than in-plane expansion.<sup>29</sup> This characteristic is not the focus of this study, but it would be expected to influence phenomena such as nucleation,<sup>7</sup> which plays a role in producing the peak in the chronoamperograms of anion transporters. Nucleation has not been observed in PPy(DBS); instead, a uniform cation-ingress front is seen<sup>31,35,36</sup> (which for modeling purposes could be considered as a single nucleus).

Only one predominantly cation-transporting system has been studied previously: PPy(*p*-toluenesulfonate), or PPy(pTS), cycled in propylene carbonate containing LiClO<sub>4</sub>.<sup>20</sup> Unlike in anion-transporting polymers, ESCR manifested itself as a small shoulder on a decaying cathodic current. The anodic current decayed smoothly (see Figure 21b for an example plot).

**1.4. ESCR Model.** According to the ESCR model, relaxation (chain opening) is governed by an Arrhenius law:<sup>20</sup>

$$\tau_r = \tau_0 e^{\Delta H/RT} \quad (1)$$

where  $\tau_r$  is the time it takes for the relaxation,  $\tau_0$  is a time constant, and  $\Delta H$  is the molar enthalpy. This energetic term depends on the applied potentials through

$$\begin{aligned} \Delta H &= \Delta H^* + \Delta H_c - \Delta H_r \\ \Delta H &\sim z_c \eta_c - z_r \eta_r \end{aligned} \quad (2)$$

where the first term  $\Delta H^*$  is the molar conformational energy consumed in the absence of electric fields and has been determined to be on the order of 10–30 kJ/mol in various polymers.<sup>8</sup> The second term  $\Delta H_c$  is the increment of conformational energy due to the closure and packing of the polymer matrix. It is proportional to the compaction overpotential  $\eta_c = E_c - E_s$ , in which  $E_c$  is the applied compaction potential and  $E_s$  is the closure potential, defined as the voltage at which the matrix begins to close. (When comparing with prior work, it is important to keep in mind that for predominantly cation-exchanging materials, such as PPy(DBS), the compaction overpotential is an anodic, rather than a cathodic, overpotential.) In other words, the higher the compaction overpotential that is applied prior to the reduction step, the higher the molar enthalpy and thus the longer the relaxation time  $\tau_r$  during reduction. The third term  $\Delta H_r$  is the electrochemical energy that contributes to matrix relaxation. It is proportional to  $\eta_r = |E_r - E_0|$ , where  $\eta_r$  is the relaxation (in this case cathodic) overpotential,  $E_r$  is the reduction potential, and  $E_0$  is the potential at which reduction begins (and the structure starts to open). So, the higher the potential that is applied during reduction, the lower the molar enthalpy, and the faster the conformational relaxation will take place. The constants  $z_c$  and  $z_r$  correspond to the charge required to compact or relax 1 mol of polymer segments, respectively.

According to the ESCR model, the time spent holding the polymer at the compaction potential, denoted as  $t_{\text{wait}}$ , also affects the molar enthalpy through  $z_c$ :<sup>13</sup>

$$z_c = z_c^0 + \frac{RT\alpha}{\eta_c} \ln t_{\text{wait}} \quad (3)$$

where  $z_c^0$  includes only potential-related contributions. The longer the time  $t_{\text{wait}}$  that the polymer is allowed to compact (at the

anodic potential for PPy(DBS)), the greater the amount of energy that is required to relax the polymer segments and the higher the molar enthalpy.

In PPy(pTS), the position of the shoulder, in time, as a function of the reduction potential was estimated by taking the second derivative of the chronoamperogram. This time,  $t_{\text{ESCR}}$ , had the expected logarithmic dependence

$$\ln(t_{\text{ESCR}}) = C' - z_r \eta_r / RT \quad (4)$$

consistent with the ESCR model. The constant  $z_r$  was calculated to be 2400 C/mol, comparable to values found for anion-transporting materials.<sup>8</sup> The occurrence of shoulders rather than peaks is probably due to the fact that the material always contains charges (PPy<sup>n+</sup>(pTS<sup>-</sup>)<sub>n</sub> in the oxidized state and PPy(pTS<sup>-</sup>·Li<sup>+</sup>)<sub>n</sub> in the reduced state), resulting in a significant water content at all times (since dipolar water molecules interact strongly with charged species). This would make it difficult for the polymer to reach a state of deep compaction.

In this work, we show that the behavior of PPy(DBS) is similar to that of PPy(pTS), with smooth current decays upon oxidation and small shoulders upon reduction. The shoulder occurs sooner when the reduction (relaxation) potential  $E_{\text{ca}}$  is increased. By deconvoluting the current into an exponential decay component and an ESCR peak component, the peak time is found to decrease logarithmically with  $E_{\text{ca}}$ , as expected by the ESCR model. The peak position increases logarithmically with the oxidation (compaction) potential  $E_{\text{an}}$ , and it increases with the time that  $E_{\text{an}}$  is held, also consistent with the ESCR model.

## 2. Methods

**2.1. Experiment. 2.1.1. Substrate Preparation.** The substrates on which the PPy was deposited were sections of oxidized, 500  $\mu\text{m}$  thick Si wafers coated with 30  $\text{\AA}$  of Cr and 2000  $\text{\AA}$  of Au by thermal evaporation (Cooke, 80 A,  $5 \times 10^{-6}$  Torr, 5  $\text{\AA}/\text{s}$ ). These surfaces were flat and mirror-smooth, as seen visually (see the Supporting Information) and by atomic force microscopy and profilometry.<sup>34,37</sup>

Because of the perfect smoothness of the surfaces, on clean Au the PPy delaminated during cycling, preventing the completion of the series of experiments. It is known that delamination of PPy(DBS) films from smooth Au can occur after a relatively small number of cycles.<sup>37</sup> Thus, just prior to PPy deposition, the wafer sections were immersed into a 1 mM (5 vol %) solution of  $\alpha$ -lipoic acid (Aldrich) in ethanol for 24 h to cover the Au surface with a monolayer (or more) of this organic molecule. After treatment with  $\alpha$ -lipoic acid, the wafer sections were rinsed with deionized water for 5 s just prior to PPy deposition. Treatment with  $\alpha$ -lipoic acid was based on the supposition that the monolayer would interact more strongly with the PPy than the Au does, helping to improve adhesion, and that the two thiol moieties of this molecule would stabilize the monolayer during electrochemical cycling.<sup>38</sup> (Monolayers with a single thiol are completely removed during electrochemical cycling.<sup>39,40</sup>) No delamination occurred on the treated surfaces, based on unchanging total charge and unvarying peak positions during cyclic voltammograms taken throughout the course of the experiments. (This does not, however, establish the efficacy of the treatment, since untreated samples have a wide range of lifetimes.<sup>37</sup> Further tests are required to establish that the  $\alpha$ -lipoic acid improves adhesion.)

**2.1.2. Polymerization.** The pyrrole monomer was sieved through  $\text{AlO}_2$  powder (Aldrich) before use. Polymerization was performed potentiostatically in a solution of 0.1 M pyrrole (Sigma-Aldrich) and 0.1 M NaDBS (Aldrich) in deionized water. The Au on the wafer section served as the working electrode (WE). It was immersed to a depth of 2.0 cm into the solution and held in place with a toothless Cu alligator clip (not immersed but positioned above the solution). An Autolab EcoChemie potentiostat (pgstat30) was used to apply a constant 0.46 V vs an Ag/AgCl reference electrode (BAS, Inc.). The counter electrode (CE) was a 5 cm  $\times$  2 cm  $\times$  0.5 cm porous carbon plate. The working electrode was secured  $\sim$ 4 cm from the counter electrode so that their surfaces were facing each other and parallel. The reference electrode (RE) was placed 1 cm from the working electrode. Film thickness was controlled by ending the polymerization after 100 mC/cm<sup>2</sup> of charge had been consumed, which resulted in 5000 Å thick PPy films, determined by film color.<sup>41</sup> The low voltage led to films of uniform thickness. The average current density during polymerization was 64  $\mu\text{A}/\text{cm}^2$  and remained relatively constant throughout polymerization. After PPy deposition, the wafer sections were scribed into pieces 0.5 cm wide and 3.0 cm long.

**2.1.3. Cycling.** Electrochemical cycling was done by immersing the films to a depth of 0.5 cm (for square-shaped immersed areas of 0.25 cm<sup>2</sup>) into a 0.1 M aqueous solution of NaDBS, with the electrochemical cell arranged the same way as during polymerization. The mass of the cycled PPy was estimated to be 19  $\mu\text{g}$ , using the dimensions of the film and values of PPy density reported in the literature.<sup>42,43</sup> [The effective film volume  $V$  was calculated using length = depth immersed into electrolyte = 0.5 cm, width = sample width = 0.5 cm, and thickness = 5000 Å =  $5 \times 10^{-5}$  cm, giving  $V = 1.25 \times 10^{-5}$  cm<sup>3</sup>. Using a density of 1.5 g/cm<sup>3</sup>, film mass =  $1.25 \times 10^{-5}$  cm<sup>3</sup>  $\times$  1.5 g/cm<sup>3</sup> = 1.88  $\times 10^{-5}$  g.] Switching in NaDBS ensured that only cation transport took place. (In electrolytes such as NaCl,  $\text{Cl}^-$  transport occurs in parallel,<sup>44</sup> which complicates data analysis.) The cell was covered with Parafilm M (Pechiney) to prevent evaporation during the long course of the experiments ( $\sim$ 10 h). Solution pH was monitored during cycling with universal indicator strips (EMD colorpHast); the solution was replaced if the pH drifted more than one unit from neutral.

Cyclic voltammetric (CV) scans were performed between  $-1.0$  and  $+0.4$  V at 25 mV/s vs Ag/AgCl. Chronoamperometric scans (CAs) were performed using a programmed potential stepping routine, which applied alternating anodic and cathodic potential steps, each of 5 s duration (Figure 2). Anodic potentials were first varied in a series, incrementally from  $-0.2$  to  $+0.4$  V, by 0.05 V. Note that all of these potentials were above the oxidation peak. A constant cathodic potential step was applied between each anodic step. The anodic potential series was repeated for incrementally increasing cathodic potentials in steps of 0.05 V from  $-0.7$  V (within the region of the reduction peak) to  $-1.4$  V (at which hydrolysis occurs). Two CV scans were performed before each CA series, both to ascertain the state of the PPy film and to “erase” any memory effects that may have been induced by the sequence. The entire process was completed separately on three samples, varying the cathodic potentials in the opposite direction (from  $-1.4$  to  $-0.7$  V) on one sample (sample 2). The order did not affect the results. In the results, representative data from only one sample are presented; to see results from all three samples, please refer to the Supporting Information.

In holding time experiments, the potential was switched between a fixed cathodic potential,  $-1.0$  V held for 5 s, and a

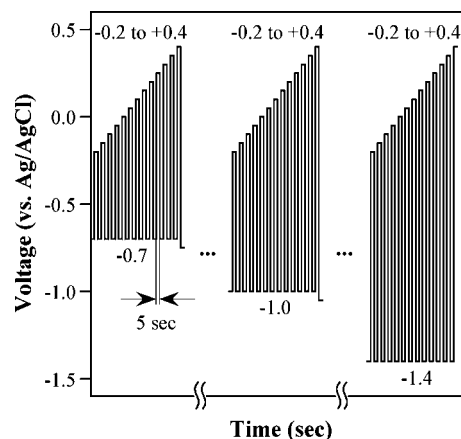


**Figure 2.** Illustration of the series of potentials that were applied during chronoamperometry. Voltages were stepped from a given cathodic potential, held for 5 s, to a series of anodic potentials between  $-0.2$  and  $+0.4$  V in increments of 0.05 V, also held for 5 s. Two cyclic voltammograms were then performed between  $+0.4$  and  $-1.0$  V, the cathodic potential was lowered by 0.05 V from the previous series of steps, and the series repeated. Stepping to only three cathodic potentials is illustrated, with the remaining ones and the CVs represented by ellipses, “...”.

fixed anodic potential, 0.0 V, held for increasingly longer times: 1, 2, 5, 10, 20, 50, 100, 200, 500, and 1000 s. These experiments were also repeated on three samples.

During electrochemical switching, no evidence of nucleation was observed. [Because PPy is electrochromic, the switching reaction can be monitored visually as a color change. Nuclei thus appear as small spots of a different color that grow outward and coalesce.] The Au surfaces were smooth down to the nanometer level, giving the PPy great homogeneity, with no preferred nucleation sites. There was, however, visual confirmation of fast lateral ion transport from the edges of the sample toward the center. This occurred simultaneously with a color change at the center of the film due to vertical ion transport from the electrolyte/film interface toward the electrode. This is well-known in PPy(DBS) and is due, as mentioned above, to its lamellar microstructure.<sup>33,45</sup>

**2.2. Data Analysis. 2.2.1. Anodic Chronoamperograms.** To quantify the speed of the oxidation reaction, stretched exponential curves were fit to the anodic chronoamperograms (Figure 3). (This choice is discussed in the Supporting Information.) The stretched exponential function is given by<sup>46,47</sup>

$$I = I_0 e^{(-t/\tau)^\beta}, \quad 0 < \beta \leq 1 \quad (5)$$

where  $I$  is the current,  $I_0$  is the initial current,  $\tau$  is a relaxation time (not the same as  $\tau_r$  in eq 1),  $t$  is the elapsed time, and  $\beta$  is the stretching coefficient. Stretched exponentials have been used to fit a range of relaxation behaviors, with  $\beta$  being an empirical value.<sup>48</sup> Of relevance to its use here with PPy redox, such a function can be used to describe a system with a distribution of relaxation times, for example due to different local environments or conjugation lengths.

Stretched exponentials have previously been fit to the CAs of conjugated polymers when the redox process is not under conformational relaxation control (i.e., to the cathodic current decays in anion-transporting materials).<sup>8</sup> It should be noted that when  $\beta = 1$ , such a fit corresponds to the ESCR model in the absence of conformational relaxation control.<sup>7</sup>

$$I_d(t) = bQ_d e^{-bt} \quad (6)$$

where  $b$  is a constant related to the diffusion coefficient inside the swollen film and  $Q_d$  is the charge consumed during diffusion kinetic control.

In the stretched exponential function in eq 5,  $I_0$  was set equal to the initial current, which was the current at  $t = 0.20$  s. Values prior to this were discarded in both the anodic and cathodic steps because during this time, there was capacitive charging of the Au (see Figure 5). The values for  $\tau$  and  $\beta$  were determined through an iterative process using a Matlab script. The best fitting combination was deemed to be the one that resulted in the smallest rms error  $\varepsilon$ , where  $\varepsilon$  is the sum of the differences between the data points of the experimental curve and the fit between  $t = 0$  and 5 s. The data could be well fit ( $\varepsilon < 0.01$ ) using just two values of  $\beta$ :  $\beta = 0.95$  for anodic voltages  $-0.15 \text{ V} < E_{\text{an}} < 0 \text{ V}$  and  $\beta = 0.85$  for  $E_{\text{an}} > 0 \text{ V}$ . (The two values might arise from moving from the electrochemical reaction that takes place in Gaussian 2 to the pseudocapacitive process which occurs above that; see Figure 4. These two reactions may have different time constants. For example, two different kinetic processes, with different kinetic coefficients, are obtained during the oxidation of poly(3-methylthiophene).<sup>49</sup>)

**2.2.2. Cathodic Chronoamperograms.** The shoulders in the cathodic chronoamperograms of PPy(DBS) were even smaller than those for PPy(pTS).<sup>20</sup> Thus, the method of locating the peak position by taking the second derivative of the curve could not be used. To examine the nature of the current component that gave rise to the shoulders in the cathodic CAs, these curves were also fit with exponentials

$$I = I_0 e^{-t/\tau} \quad (7)$$

but these were not stretched (i.e., they had  $\beta = 1$ ). (There were not always sufficient data on either side of the shoulder to allow an accurate determination of  $\beta$ , and using  $\beta = 1$  gave good results, with  $\varepsilon < 0.01$ .) To ensure that the fit matched the initial current density, the curve was constrained to intersect with the first considered experimental data point at  $t = 0.20$  s. At potentials more cathodic than  $-1.0 \text{ V}$ , at which the shoulder was clearly evident, the exponential was fit only to the sections of the curve before and after the shoulder (denoted  $\Gamma_1$  and  $\Gamma_2$ , respectively, in Figure 3b). As the shoulder grew or moved to shorter times,  $\Gamma_1$  shrank to zero.

Fitting of  $\tau$  was done by starting with large  $\Gamma_1$  and  $\Gamma_2$  (in the extreme case, covering the entire CA) and incrementally decreasing their size until the rms error of the fit in both of those regions reached a steady minimum value. Too large a  $\Gamma_1$  required the exponential to pass through the shoulder, thus making it decay too slowly and introducing a large rms error in the region of  $\Gamma_2$ . Likewise, too large a  $\Gamma_2$  also required the exponential to pass through the shoulder, again making it decay too slowly and introducing a large rms error in the region of  $\Gamma_1$ . Incrementally reducing  $\Gamma_1$  and  $\Gamma_2$  until the error no longer decreased forced the exponential to fit only the portions of the CA away from the shoulder, while at the same time keeping  $\Gamma_1$  and  $\Gamma_2$  as large as possible to ensure the most accurate fit to the exponential. The fitted exponential was then subtracted from the original data, revealing what we shall refer to as the ESCR peak (dotted line in Figure 3b).

### 3. Results

**3.1. Cyclic Voltammetry.** The end-point potentials used during the chronoamperometric studies were chosen based on cyclic voltammograms. CVs also provided a means of monitoring film electroactivity and adhesion and provided insight for understanding the CA results.

Typical CVs for PPy(DBS) and a clean Au surface are shown in Figure 4a. The largest oxidation and reduction peaks of the PPy occur at approximately  $-0.40$  and  $-0.45 \text{ V}$  vs Ag/AgCl, respectively. Shoulders are visible for both processes at  $-0.55$  and  $-0.65 \text{ V}$ . The processes associated with the oxidation peak are essentially complete at  $-0.2 \text{ V}$ , indicated by a leveling-off of the current. (The origin of the constant, so-called “capacitive” current above this peak, seen here between  $-0.2$  and  $+0.4 \text{ V}$ , has been attributed to a variety of causes and is still the subject of controversy. The magnitude of this current in PPy(DBS) has been shown to be highly dependent on the polymerization conditions, being entirely absent in some cases.<sup>50</sup>) The reduction processes are complete by  $-0.90 \text{ V}$ , and the large cathodic current beyond  $-1 \text{ V}$  is due to hydrolysis. The ranges of end-point potentials used in the CA experiments are indicated by the hollow arrows. Note that the anodic end-point potentials are all above both oxidation peaks, and the cathodic potentials are all below the first reduction peak.

The CVs from the three samples that were tested all showed identical peak positions after 10 break-in cycles. It should also be noted that there was no noticeable cathodic shift of the reduction peaks due to compaction upon cycling to  $+0.4 \text{ V}$ ,

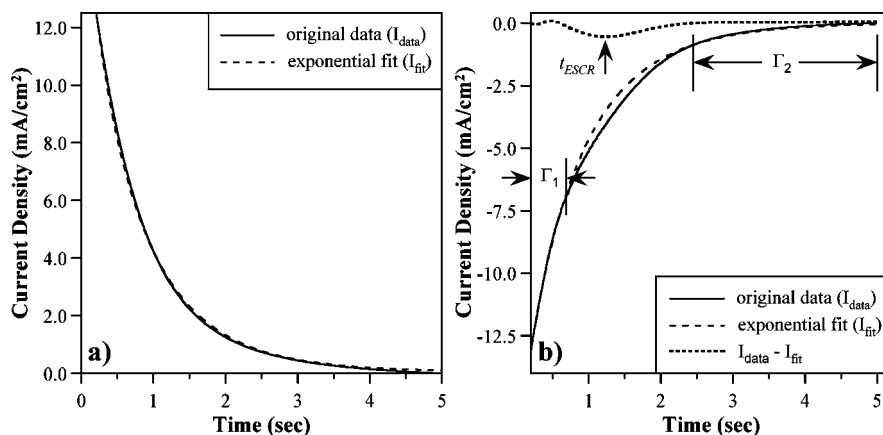


**Figure 3.** (a) Stretched exponential curve fit (dashed line) to an anodic CA (solid line), in this case a step from  $-1.40$  to  $+0.10 \text{ V}$ ;  $\beta = 0.85$ . (b) Exponential curve fit to the beginning and end of a cathodic CA, in this case a step from  $+0.40$  to  $-1.00 \text{ V}$ . The difference between these curves (dotted line) is also indicated; this is termed the ESCR peak, and the time at which the peak occurs is  $t_{\text{ESCR}}$ .

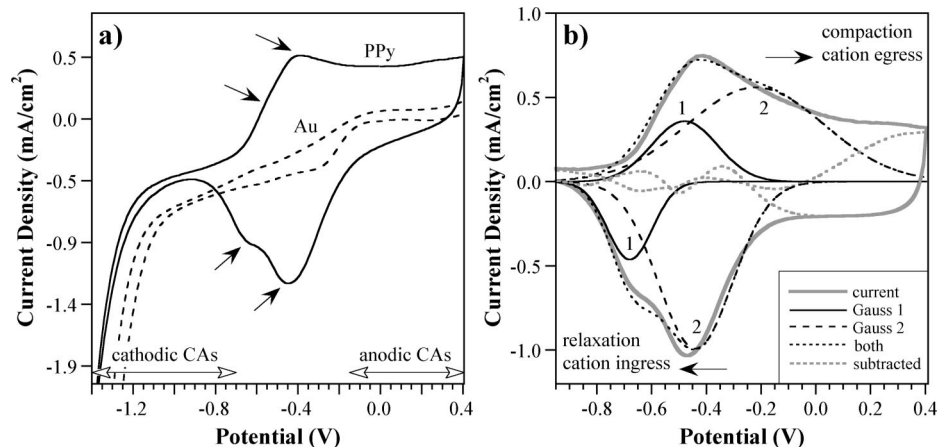


**Figure 4.** (a) Equilibrated cyclic voltammogram taken at 25 mV/s of a 5000 Å thick PPy(DBS) film and of an uncovered Au film. Solid arrows point to the two pairs of oxidation and reduction peaks, one of which is seen only as a small shoulder. (b) The PPy CV after it was corrected for IR drops and dual Gaussian curve fits to the peaks. The charge densities under Gaussian peaks 1 and 2 are 1.08 and 3.46 mC/cm<sup>2</sup>, respectively.

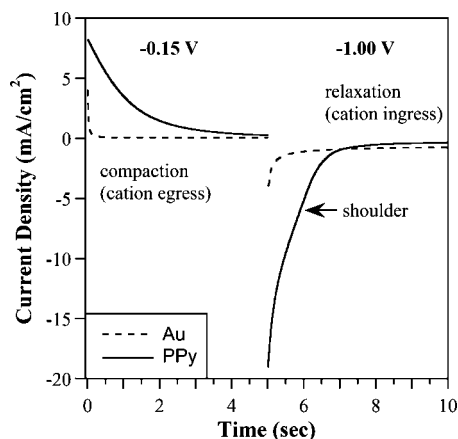


**Figure 5.** Typical chronoamperograms, before subtraction of baseline currents, for PPy(DBS) and for Au upon stepping from  $-1.00$  to  $-0.15$  V and back again. Each potential was held for 5 s.

compared to the peak positions when cycling to an upper voltage limit of only  $-0.2$  V.

The two pairs of peaks in the CV can be approximated by two pairs of Gaussians that have been constrained so that the charge in each Gaussian of the pair is equal.<sup>35</sup> Such a dual Gaussian curve fitting is shown in Figure 4b after the CV was corrected to remove IR drops.<sup>34</sup>

Previously, both color and volume change in PPy(DBS) have been found to be associated only with the smaller, more negative pair of peaks, “Gaussian 1”,<sup>35</sup> which consume only  $\sim 20\%$  of the total charge. The primary charge-consuming process represented by “Gaussian 2” is still not clear. The so-called capacitive charge is the charge that remains after subtracting the two Gaussians from the original CV.

During chronoamperometry, the currents from all the electrochemical processes that are capable of occurring at that potential flow simultaneously. It is therefore more difficult to characterize each component of the total CA current separately.

**3.2. Chronoamperometry: Overview.** A typical CA is shown in Figure 5. The anodic step (positive current) causes the oxidation reaction to occur, with corresponding cation egress, while the cathodic step (negative current) reduces the film and leads to cation ingress. The current levels off by or before 5 s, indicating the completion of the switching process.

The CA data were processed by subtracting the baseline current that continued to flow after the reduction process was

complete; this was  $0.10$ – $0.35$  mA/cm<sup>2</sup> for the anodic data and  $0.26$ – $0.70$  mA/cm<sup>2</sup> for the cathodic data. During reduction, the baseline current is due to hydrolysis (see Figure 4a), since the PPy-related processes have been completed after 5 s. These currents also occurred on bare gold working electrodes, after the capacitive charging during the first 0.2 s had stopped. (As mentioned above, because of that charging, the first 0.2 s of CA data from the PPy samples were disregarded during data analysis.) The cathodic baseline currents were only half the size of the cathodic currents at the same voltage in the CVs (Figure 4). There was no significant baseline current after 5 s of oxidation. For the experiments in section 3.3.3, the magnitude of background current flowing during the waiting time (holding the voltage at 0.0 V) was thus negligible.

Just as seen in PPy(pTS),<sup>20</sup> there was a shoulder on the cathodic curve, although in PPy(DBS) the shoulder was smaller. In the following sections, we examine the voltage-dependent behavior of the CAs, beginning with the cathodic step, during which conformational relaxation is observed, and then going on to the anodic step, which is relevant to the memory effect.

**3.3. Chronoamperometry: Cathodic Currents.** Since this paper is concerned with conformational changes, the experiments were designed to establish a particular state of the polymer matrix prior to electrochemical switching and to keep other variables constant. However, in this first set of experiments, since the cathodic potential is varied, the results also reflect the effect of faster ion migration under higher electric fields. This is unavoidable: these effects cannot be separated in this type of experiment. However, in the last set of experiments (section 3.3.3), in which the time that the polymer is held at the anodic potential prior to switching is varied and the voltage end points are kept constant, these effects can be separated. Likewise, the variation of film conductivity from the oxidized to reduced state may contribute to deviations from the exponential decay of the current; these contributions are also eliminated in section 3.3.3. The experimental protocol was designed to provide evidence that, *when all the data were taken together*, would either support or refute the ESCR model in PPy(DBS).

The cathodic currents are expected to reflect conformational relaxation since the polymer starts from a compacted state and must expand to allow cation ingress. As explained in section 2.2.2, because of the presence of shoulders, the cathodic curves were analyzed in terms of both an exponential and a subtracted component. Results are first presented as a function of cathodic potential.

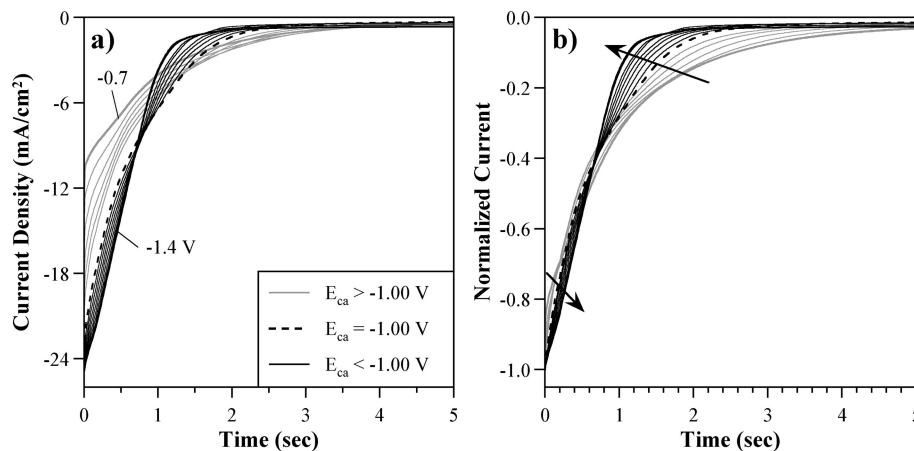


**Figure 6.** (a) Unprocessed cathodic chronoamperograms for a series of increasingly cathodic applied potentials, stepping from one anodic potential (+0.40 V held for 5 s). Potentials less negative than  $-1$  V are indicated by gray lines and those more negative by black lines. The first and last scans of the series are indicated by heavier lines. (b) Same data, normalized by the current at  $t = 0.0$  s. The arrows indicate more negative  $E_{ca}$ .

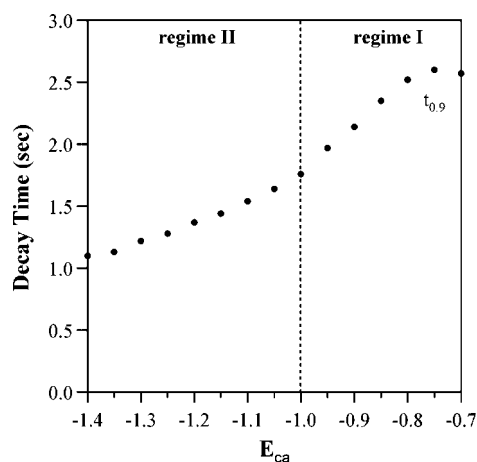


**Figure 7.** Time required for the cathodic current to drop to 10% of its initial value as a function of  $E_{ca}$ . In regime I, the reduction level of the polymer is increasing, while in regime II it has reached the fully reduced state and changes no further.

**3.3.1. Role of Cathodic (Relaxation) Potential.** The evolution of the cathodic CAs with increasingly cathodic potential  $E_{ca}$ , from  $-0.7$  to  $-1.4$  V, is shown in Figure 6a. All the currents reached a constant value before  $t = 5$  s. As expected from the CV, the currents increased with  $E_{ca}$  up to  $E_{ca} = -1.0$  V (gray lines, regime I) but increased little further for more negative potentials (black lines, regime II). In addition, with increasing cathodic potential a shoulder emerged and evolved, changing the shape of the overall curve. The relative time responses are best seen by normalizing the curves to the current at  $t = 0$  s (Figure 6b). Overall, the reaction increased in speed with  $E_{ca}$ .

Figure 6b shows that one can increase the speed of the reduction reaction by increasing the cathodic potential. Most of the increase in speed came from shortening the “tails” of the curves, which were much longer for smaller  $E_{ca}$ . The time  $t_{0.9}$  required for the current to decay to 10% of its initial value is shown in Figure 7. With increasing cathodic potential, the reaction speeded up considerably, from 2.6 to 1.1 s in going from  $-0.8$  to  $-1.4$  V based on this measure. This result is consistent with models of ion transport based on diffusion and drift,<sup>32,36</sup> which show that reduction is dominated by ion migration in the polymer and is thus responsive to changes in voltage. In regime II, beyond the reduction peak, the time decreased almost linearly with  $E_{ca}$ , suggesting that one can switch even faster with larger  $E_{ca}$ . Prior work has, however, shown that the speed plateaus beyond  $-1.6$  V.<sup>31</sup>

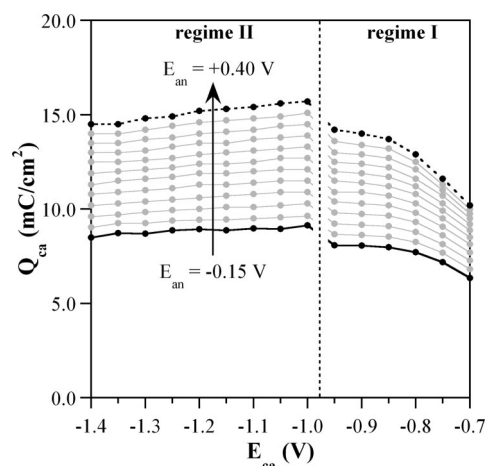


**Figure 8.** Absolute value of the total uncorrected cathodic charge as a function of cathodic potential.

There was no increase in the cathodic charge  $Q_{ca}$  consumed by the PPy (Figure 8) beyond  $-1.0$  V. Since the same change in volume is achieved upon switching a PPy(DBS) actuator to  $-1.0$  V as to  $-1.4$  V,<sup>35</sup> these data suggest that one could achieve the reduced switching time with a modest decrease in actuator efficiency. (Efficiency is defined as the mechanical work output, which stays the same, divided by the energy input, which increases linearly with the voltage times the charge.)

To illustrate the evolution of the CAs, exponential curve fits and the ESCR peaks that resulted from subtracting those fits from the data are shown for two different  $E_{ca}$  in Figure 9a. Only those curves starting from various anodic potentials and stepping to  $E_{ca} = -0.70$ ,  $-0.75$ , and  $-0.80$  V could be well fit with an exponential alone: note that the subtracted component of the  $E_{ca} = -0.70$  V curve in Figure 9a is negligible. All the other curves yielded ESCR peaks of increasing size as the cathodic potential increased, as illustrated in Figure 9b, indicating that a greater number of ions encountered compacted material. Note that “increasing  $E_{ca}$ ” in this figure, and in all subsequent figures, means increasingly large cathodic voltages, i.e., going in the direction from  $-0.70$  to  $-1.40$  V. In addition, the ESCR peak position  $t_{ESCR}$  moved to shorter times, indicating that conformational relaxation occurred more quickly. Note that as  $E_{ca}$  increased,  $\Gamma_1$  approached zero, so that for  $E_{ca} < -1.05$  V only the single point  $t = 0.2$  was fit in front of the ESCR peak. There was, however, a reasonably long stretch  $\Gamma_2$  from which to obtain  $\tau$ . Nevertheless, there may be some

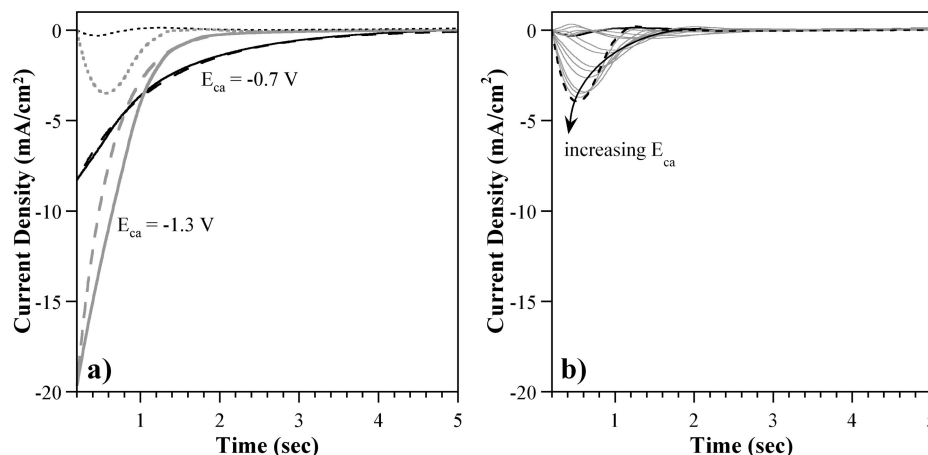


**Figure 9.** (a) Corrected CA data (solid curves), exponential fits (dashed lines), and subtracted (ESCR) components (dotted lines) for a low (black) and a high (gray) cathodic potential, both stepping from  $E_{an} = +0.40$  V. (b) ESCR components for the whole range of increasingly cathodic potentials, again stepping from  $E_{an} = +0.40$  V. The curves for  $E_{ca} = -0.7$  V (solid line) and  $-1.30$  V (dashed line), shown in (a), are highlighted in black.

uncertainty in  $\tau$  for  $E_{ca} < -1.05$  V. The fits are further discussed in the Supporting Information.

The fact that more of the current was affected by conformation relaxation as  $E_{ca}$  increased but that the relaxation occurred more quickly might seem contradictory. However, as  $E_{ca}$  goes up, the ions move more quickly (due to faster migration). One can therefore reason that a greater number of them therefore enter the polymer before it has had a chance to relax and must then wait for ESCR before they can move further, thus contributing to the peak. At lower  $E_{ca}$ , on the other hand, the relaxation may be largely complete before the bulk of the ions arrive. At the same time, higher  $E_{ca}$  provides more energy for the conformational relaxation, speeding it up.

At this point, it is important to note that it is not entirely clear how the currents in the cyclic voltammograms correspond with those in the chronoamperograms. Specifically, it is not known if (1) the ESCR peak is associated with Gaussian 1 and the exponential peak is associated with Gaussian 2 and the so-called capacitive current or (2) if instead all the current components identified on the CV contribute to both the exponential decay and the ESCR peaks. Case 1 is more likely because the charge under Gaussian 1 and the ESCR peak are of comparable magnitude and because it is reasonable to suppose that ion transport associated with strain requires chain conformation (strain has previously been shown to be associated with Gaussian 1<sup>35</sup>). Until comparable experiments are done with actuators and/or electrochromic devices, the significance of the exponential current cannot be determined. Such experiments will, however, be complicated by the two types of cation transport that occur simultaneously in PPy(DBS): fast lateral ion transport from the edges of the film to the center (due to ion transport parallel to the PPy chains along the DBS lamellae) and slower vertical ion transport from the surface toward the electrode (due to ion transport through the PPy chains).<sup>4</sup> In fact, it is also possible that the lateral transport is associated with the exponential current component, and that the vertical transport is associated with the ESCR peak. These questions must be deferred for the present.

As discussed in the Introduction, during redox a number of the properties of the polymer change, most notably its electrical conductivity. It might be argued that the shoulder on the cathodic CA is due to one of these other things. The change in electrical conductivity can, however, be ruled out based on our charge transport modeling,<sup>32</sup> which takes changes in conductivity into

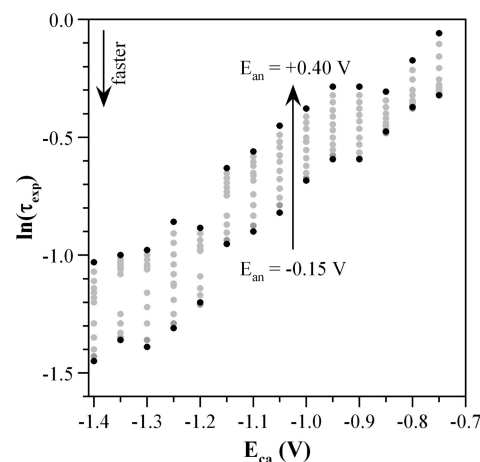


**Figure 10.** Natural logarithm of the time constants  $\tau$  for the exponential curve fits to the cathodic CAs plotted as a function of cathodic potential upon stepping from different preapplied anodic potentials.

account: no shoulder appears on the simulated CAs. Furthermore, as we show in the remaining sections of this paper, all the data are consistent with ESCR; competing theories would likewise need to account for the totality of the experimental observations.

The next two sections examine the speed and magnitude of the exponential decay and ESCR processes in more detail, but it is clear from Figures 6b and 9b that both become faster with  $E_{ca}$ . This is consistent both with greater velocities of charge migration into the polymer under higher cathodic voltages as well as with increasingly fast polymer relaxation as expected from the ESCR model.

In the following analysis of the ESCR processes, in some cases only data obtained from stepping to cathodic potentials greater than  $-1.0$  V are used, since the film is not fully reduced until that point. Steps to less negative voltages (gray lines in Figure 6) do not take the polymer to the same state, and therefore the results cannot be fairly compared. In examining the exponential decay processes, all the data have been shown, but the difference in final states of the polymer should be borne in mind.

**3.3.1.1. Exponential Curve Time Constant.** To quantify the increase in speed of the exponential decay component of the current during reduction, the log of the time constants  $\tau$  (see eq 6) of the exponential fits was plotted vs  $E_{ca}$  (Figure 10). (Additional plots are shown in the Supporting Information.) Smaller values of  $\tau$  correspond to faster switching. The time

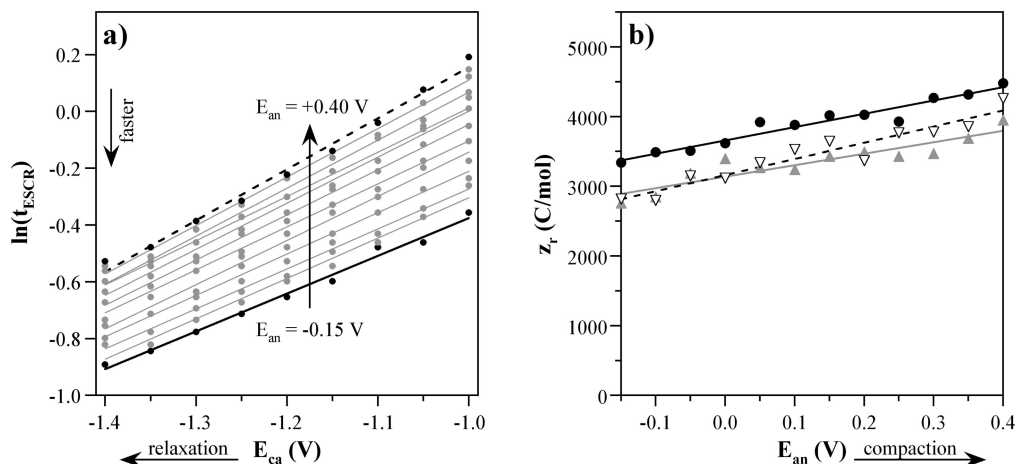


**Figure 11.** (a) Log of the ESCR peak position as a function of cathodic potential for different anodic potentials. (b) Charge  $z_r$  required to relax 1 mol of polymer segments, with the filled black symbols showing the data obtained from (a) and the other two symbols showing data obtained from the other two data sets. (Correlation coefficients  $R$  were 0.968 for the filled circles, 0.955 for the empty triangles (dashed black line), and 0.914 for the gray triangles (solid gray line).)

constant of the exponential process decreased strongly with  $E_{\text{ca}}$  (i.e., with increasingly negative  $E_{\text{ca}}$ ), consistent with both the ESCR model and with faster migration under higher electric fields. The  $\tau$  also depended on the previously applied  $E_{\text{an}}$ , increasing somewhat as  $E_{\text{an}}$  was raised (indicated by the arrow). This is discussed below.

**3.3.1.2. ESCR Peak Position.** We now turn to the “subtracted” peak. As shown in Figure 9b, the ESCR curve peaked sooner with increasing cathodic potential. The ESCR model (eq 4) predicts that  $t_{\text{ESCR}}$ , the peak time, should have a logarithmic dependence on  $E_{\text{ca}}$ . It does, as shown in Figure 11a. The fits are good (correlation coefficients  $R$  were between 0.986 and 0.996), consistent with conformational relaxation kinetics controlling the reaction process represented by this current component, with faster conformational relaxation under larger cathodic overpotentials.

The intercepts of the lines in Figure 11a increased with  $E_{\text{an}}$ , showing that the initial state of the polymer affects the speed of ESCR, with higher  $E_{\text{an}}$  producing a more compact matrix, and thus increasingly time-delayed peaks. A greater amount of energy is therefore required to open the structure in the same time.

The slopes of the lines in Figure 11a were used to obtain the constants  $z_r$ , which quantify the charge required to relax 1 mol of polymer segments from eq 4, shown again here for ease of understanding:

$$\ln(t_{\text{ESCR}}) = C' - z_r \eta_r / RT$$

Correlating eq 4 with Figure 11a,  $C'$  represents the y-intercept of the lines,  $\eta_r = (E_0 - E_r)$  represents the independent variable (on the x-axis, where  $E_r = E_{\text{ca}}$  is the cathodic reduction potential), and  $z_r/RT$  represents the slope of the lines.  $E_0$  is the potential at which reduction begins. Based on the total current in the cyclic voltammogram in Figure 4,  $E_0 = -0.2$  V, but based on Gaussian 1,  $E_0 = -0.5$  V. The latter value agrees with the one previously observed for the onset of higher lateral mobility in PPy(DBS) due to matrix opening (see Figure 14 in ref 31). The value chosen for  $E_0$  does not affect the calculation of  $z_r$ . The ideal gas constant  $R$  and the temperature  $T$  were taken as 8.314 J/(K mol) and 300 K, respectively, giving  $RT = 2494$  J/mol. Under these assumptions,  $z_r$  was calculated by multiplying the slope of the lines by  $RT$ . [For the purpose of the calculation,

the signs of the slopes were reversed because of the way the compaction potential was plotted in Figure 11a, with increasing overpotentials to the left, instead of to the right as in anion transporters.]

The values of  $z_r$  found from Figure 11a and from the other two sets of data are plotted as a function of  $E_{\text{an}}$  in Figure 11b. They begin at 2800–3500 C/mol for initial  $E_{\text{an}} = -0.15$  V and increase to 3800–4500 C/mol for initial  $E_{\text{an}} = 0.40$  V. Increasing  $z_r$  with increasing compaction overpotentials was expected from the model and from prior experimental results with other conjugated polymers. As has been found previously, the higher the degree of closure of the matrix, the more sensitive the opening of the structure is to the electric fields.<sup>6</sup>

**3.3.2. Role of Anodic (Compaction) Potential.** We now examine the effect of the anodic (compaction) potential on the subsequent cathodic chronoamperograms, which are expected to be strongly influenced by ESCR. A series of chronoamperograms were taken upon stepping to fixed cathodic potentials from different initial anodic potentials; each potential, anodic and cathodic, was held for 5 s (Figure 2). As shown in Figure 12a for the fixed  $E_{\text{ca}}$  of  $-1.40$  V, with increasing  $E_{\text{an}}$  the cathodic current curves shifted to the right (longer reaction completion times) and slightly down (somewhat higher initial currents). The higher currents were expected due to the greater quantity of charge that must be exchanged when starting at higher  $E_{\text{an}}$ , as seen in the cyclic voltammograms.

Using the time for the current to decay to 10% of its initial value  $t_{0.9}$  as a measure of the reaction time, the time is found to be linear with increasing  $E_{\text{an}}$ . Thus, while increasing  $E_{\text{an}}$  causes the anodic step to go faster (by 0.5 s in going from  $-0.15$  to  $+0.40$  V; see section 3.4.1), it also causes the subsequent cathodic step to go slower (by 0.4 s over the same range). The benefits of a faster anodic step are therefore canceled by a slower subsequent cathodic step. To gain speed overall, a carefully shaped waveform would be needed that would spike the voltage initially and then drop it to prevent the polymer from reaching a deep level of compaction.

Exponential curve fits and the ESCR peaks that resulted from subtracting those fits from the data are shown for a low and a high  $E_{\text{an}}$  in Figure 13a. Like the CA curves from which they were derived, the exponential fits decayed more slowly as  $E_{\text{an}}$  was increased (shown in the Supporting Information). Figure 13b shows that the ESCR peaks increased in magnitude (more

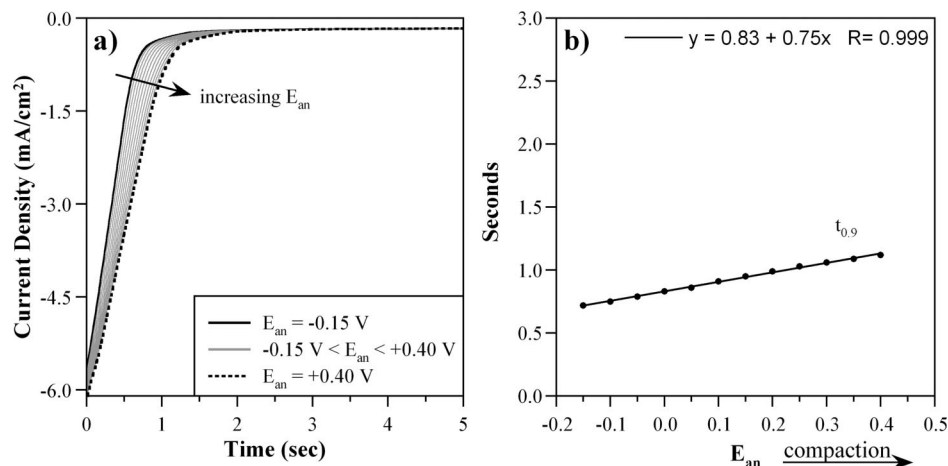


**Figure 12.** (a) Cathodic chronoamperograms for a series of preapplied anodic potentials  $E_{an}$  upon stepping to one cathodic potential ( $-1.40$  V vs Ag/AgCl). (b) Time required to reduce the cathodic current to 10% of its initial values as a function of  $E_{an}$ .

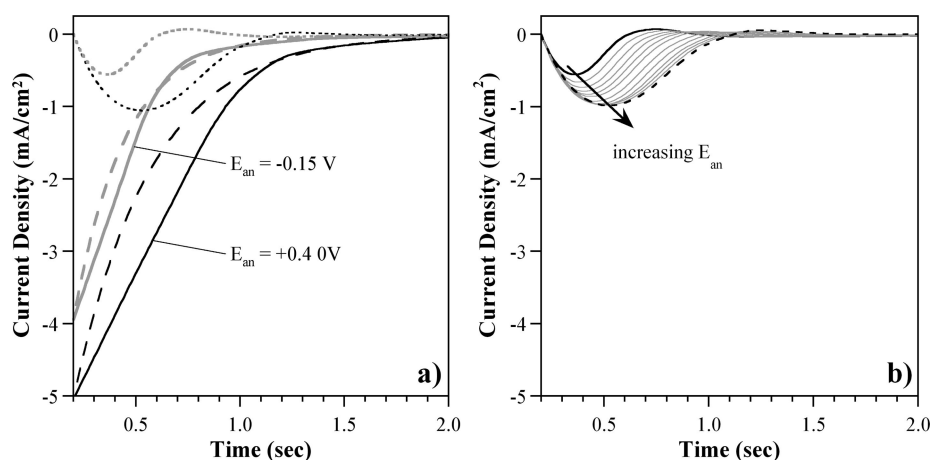


**Figure 13.** (a) Exponential (dashed lines) and ESCR (dotted lines) components of the cathodic current (solid lines) upon stepping to  $E_{ca} = -1.40$  V from high and low initial anodic potentials. (b) ESCR components for the whole range of increasingly anodic prepotentials, again stepping to  $E_{ca} = -1.40$  V. The highlighted curves for  $E_{an} = -0.15$  V (solid black line) and  $+0.4$  V (dashed black line) are shown in (a).

of the polymer was compacted, so more of the current was affected) and also that the positions of the peak shifted to longer times (ion transport must wait longer for matrix relaxation to occur). These results lend additional support to the hypothesis that these peaks arise from conformational relaxation processes.

We now examine the ESCR time dependences in more detail. (The time constants obtained from the exponential fits are shown in the Supporting Information; there is a small increase in  $\tau_{exp}$  with  $E_{an}$  for reasons that are not yet understood, since only the ESCR peak is expected to reflect compaction.) For  $E_{ca}$  that were less negative than  $-0.80$  V, no clear “subtracted” curve existed, regardless of the initial  $E_{an}$  that was applied, perhaps because chain relaxation is not rate-limiting at those potentials (for example, because slow ion transport velocities are rate-limiting instead). It is also possible that there were no ESCR peaks because these overpotentials are not high enough to reduce the fraction of the material that has been compacted. (Under these  $E_{ca}$ , the polymer is not completely reduced, as seen in the cyclic voltammograms and reflected in the lower charge exchanged.) If no electrons are added to the compacted material because higher energies are required to put the electrons there than onto noncompact material, then the cations have no reason to enter the compacted material, and no ESCR peak would be produced. It would be consistent with the ESCR model to postulate that the compacted material requires higher overpotentials  $\eta_c$  to be reduced. This would also be consistent with a relationship between Gauss 1 (Figure 4b) and the ESCR peak.

In the plots presented below, even though ESCR peaks existed for  $E_{ca} = -0.85$ ,  $-0.90$ , and  $-0.95$  V, only data taken at or below  $-1.0$  V were used so that comparisons were made of the polymer in the same fully reduced final state. This allowed us to examine how ESCR processes limit ion transport, rather than looking at a mixture of effects due to different reduction levels.

According to eq 4, a log dependence of  $t_{ESCR}$  on  $E_{an}$  is expected. Figure 14a shows that this was the case: increasing anodic prepotentials resulted in logarithmically longer  $t_{ESCR}$ . The decrease in peak time with cathodic potential  $E_{ca}$  that is seen here as a downward shift of the lines was previously detailed in section 3.3.1.2.

The slopes of the curves in Figure 14a were used to calculate  $z_c$ , the amount of charge required to compact 1 mol of polymeric segments, analogously to the calculation of  $z_r$  in section 3.3.1.2. The values of  $z_c$  are shown as a function of cathodic potential in Figure 14b.

The values of  $z_c$  are less than the values of  $z_r$  (compare Figure 11b). This has usually been the case in other polymers as well. As shown in ref 18, the size of  $z_c$  and  $z_r$  are inversely linked by the strength of the interaction of the solvent with the polymer. A smaller  $z_c$  than  $z_r$  shows that there are strong polymer–solvent interactions, favoring matrix opening, so that larger compaction overpotentials are needed to close the structure (smaller  $z_c$ ), and smaller relaxation overpotentials are needed to open it to the same degree (larger  $z_r$ ).<sup>18</sup> This becomes clear from looking at

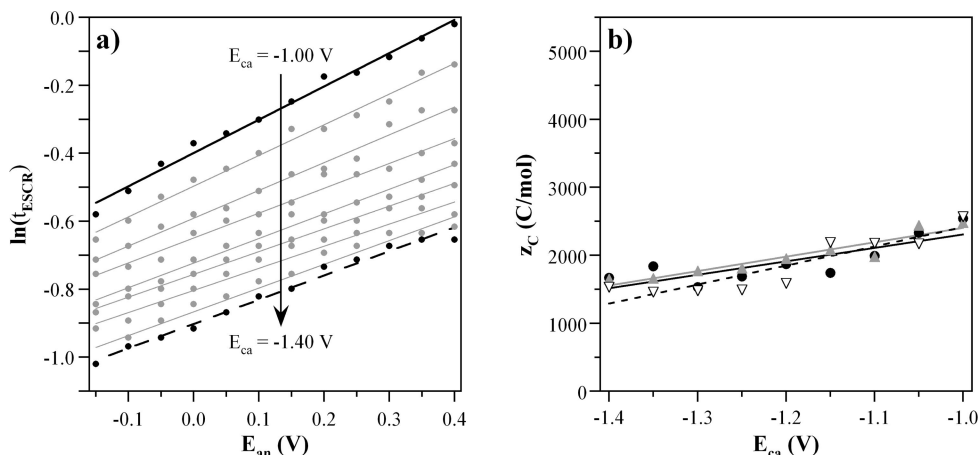


**Figure 14.** (a) ESCR peak position as a function of preapplied anodic potential for a series of cathodic potentials. (b) Charge  $z_c$  required to compact 1 mol of polymer segments, with the filled black symbols showing the data obtained from (a) and the other two symbols showing data obtained from the other two data sets.

eq 2:  $\Delta H \sim z_c \eta_c - z_r \eta_r$ . Achieving the same  $\Delta H$  given a larger  $z$  requires a smaller  $\eta$ . Strong polymer–water interactions are expected in PPy(DBS) given the fact that there are always charges in the material, as mentioned above, and these interactions are evidenced by a large increase in volume during the first reduction cycle due to permanent water ingress.<sup>34,35</sup>

The compaction constant  $z_c$  decreased with increasingly cathodic potentials, meaning that larger compaction overpotentials are needed to close the structure to the same extent. The reason for this is not clear, since within regime II the polymer matrix was not thought to change (Figure 20).

**3.3.3. Role of Anodic Holding Time (Wait Time).** In the previous sections, the direct role of the voltage on ion transport via migration could not be neatly separated from the indirect role of the voltage on ion transport via electrochemically stimulated chain relaxation. There is, however, a set of experiments that can successfully separate migration and ESCR effects: changing the holding or “wait time”  $t_{\text{wait}}$ , i.e., the time for which the polymer is held in the oxidized state before the cathodic step is applied. The longer the holding time, the more compacted the matrix becomes. Since the starting and ending potentials are the same, the migration and diffusion forces are the same. Thus, any change in the chronoamperograms can only be due to compaction and relaxation of the polymer.

The potential was held at 0.0 V to compact the polymer for times between 1 and 1000 s, and then it was stepped to  $-1.0$  V and held for 20 s. To completely “erase” the memory, two CVs were done before each oxidation step.

Figure 15 shows the cathodic CAs as a function of holding time  $t_{\text{wait}}$ . They moved toward longer times and greater total consumed charge with increasing holding time, although, interestingly, the initial current density remained unchanged.

It was not possible to accurately determine the exponential time constants for the longer holding times because of the large size and long duration of the ESCR peak. Therefore, a single time constant  $\tau$ , the one that best fit the 1 s holding time CA (which had the smallest ESCR peak, and thus the most reliable fit), was used for the exponential fits for all of these CAs. This approach assumes that the exponential current decay is unaffected by ESCR processes. If this current component is due to unimpeded diffusion/drift in an open matrix, then this assumption is reasonable. However, without accurate fits this assumption cannot be tested.

The exponential fit and the ESCR peaks for two holding times are shown in Figure 16a, while Figure 16b shows the entire

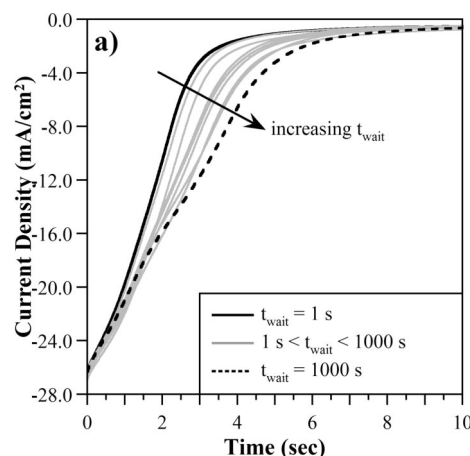


**Figure 15.** Cathodic CAs upon stepping to  $-1.0$  V after holding at 0.0 V for varying times  $t_{\text{wait}}$ .

series of ESCR peaks obtained at all the holding times. These peaks grew in size, and shifted to longer times, as the holding time was increased, consistent with the ESCR theory. In fact, this behavior cannot be accounted for in any other way than by changes taking place in the polymer as it is held in the oxidized state.

It may seem surprising that the total charge consumed during reduction increased. If our curve fitting approach to these data is reasonable, then all of this extra charge can be assigned to the ESCR peak, which is presumably associated with cation transport. Then, these data show that a greater number of cations are pulled into the polymer after longer holding times. Thus, cations must continue to be gradually expelled over time as the polymer is held in the oxidized state, bringing the film to a higher oxidation level. Experiments with actuators would be informative: is there a slow contraction commensurate in magnitude and speed with this cation expulsion (the charge increased logarithmically with  $t_{\text{wait}}$ ; this is shown in the Supporting Information) when the polymer is held in the oxidized state? (Pei’s work on PPy(DBS) bilayer actuators examined curvature drift over time in the *reduced* state.<sup>51</sup>) Elemental analysis would also help to shed light on this.

According to eq 8,<sup>14</sup> which was empirically determined and later confirmed by the ESCR model

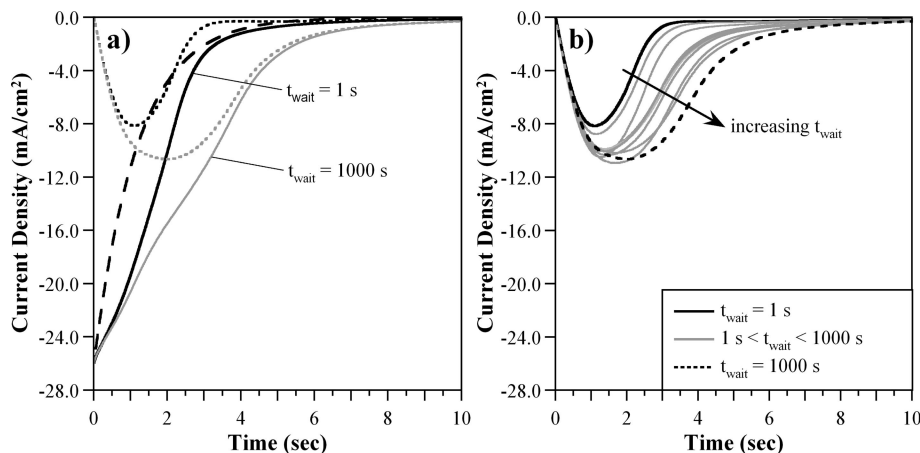


**Figure 16.** (a) Exponential curve fit (dashed line) to cathodic CAs at two different anodic holding times: 1 s (solid black line) and 1000 s (solid gray line). The ESCR peaks are denoted by the corresponding black and gray dotted lines. (b) The ESCR peaks for the whole series of holding times, with the two cases in (a) indicated in black.

$$\ln(t_{\text{ESCR}}) = C + A \ln(t_{\text{wait}}), \quad \text{equivalent to } t_{\text{ESCR}} = c(t_{\text{wait}})^A \quad (8)$$

where  $C$  and  $c$  are constants, so the log of the ESCR peak time should depend logarithmically on the anodic holding time;<sup>13</sup> this is shown in Figure 17. The relationship of  $\ln(t_{\text{ESCR}})$  with  $\ln(t_{\text{wait}})$  is indeed approximately linear. (Alternatively, plotting  $t_{\text{ESCR}}$  vs  $t_{\text{wait}}$  gives  $y = 1.2x^{0.065}$  with  $R = 0.86$ . This power law allows the data to be interpreted more easily for actuator control.)

The fact that the ESCR peak position depends on the wait time in the manner predicted by the ESCR model, in conjunction with all the data in the previous sections that is also consistent with ESCR, allows a firm conclusion that this peak is in fact due to ESCR processes. While it may be possible to explain several of the individual observations in other ways, the totality of the evidence points to ESCR.

**3.4. Chronoamperometry: Anodic Currents.** During oxidation, the polymer transitions from an expanded state to a compacted state. Since the polymer matrix begins in an open state, no conformational relaxation effects are expected. The rate of ion transport is expected to be influenced solely by the magnitude of the overpotential (since all other electrochemical variables, e.g., temperature and electrolyte concentration, are held constant). In addition to confirming this result, this section presents behaviors of the anodic currents, which provide additional insight into the kinetics and energy consumption during redox.

**3.4.1. Overview of Results.** Both the anodic potential applied during the step and the cathodic potential that had been applied before the step were examined for their impact on the current. Figure 18a shows CA curves resulting from steps to different anodic potentials  $E_{\text{an}}$  from a fixed initial cathodic potential  $E_{\text{ca}}$  of  $-1.4$  V (recall that initial cathodic potentials  $E_{\text{ca}}$  were examined throughout the range from  $-0.7$  to  $-1.4$  V, but just the one series is shown here), and Figure 18c shows CAs from different cathodic potentials  $E_{\text{ca}}$  to a fixed anodic potential  $E_{\text{an}}$  of  $+0.4$  V (again, only one series is shown, although data were collected for  $E_{\text{an}}$  from  $-0.15$  to  $+0.40$  V).

Looking at the current density in Figure 18a, the initial current  $I_0$  increased with  $E_{\text{an}}$ , from  $8.0$  to  $18.0$  mA/cm<sup>2</sup>, consistent with the CVs, which showed continued charge consumption with increasing  $E_{\text{an}}$  even above the oxidation peak. Despite these differences in  $I_0$ , however, all the currents had decayed to constant values by  $t = 5$  s.

In these thin films, we did not see a delay in the onset of oxidation due to conversion of the film from an insulating to a

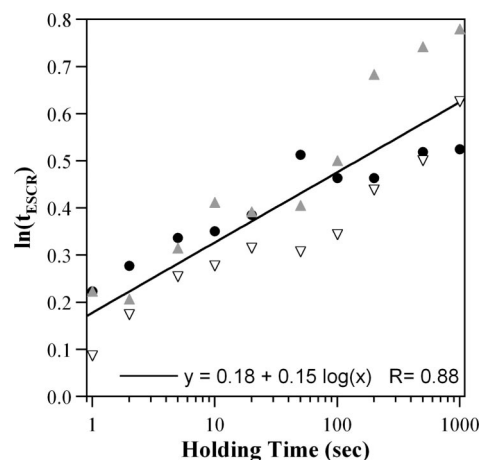


**Figure 17.** ESCR peak position as a function of anodic holding time, with the empty triangles showing the data obtained from Figure 16 and the other two symbols showing data obtained from the other two data sets. The line shows the best fit to all three sets of data.

conducting state. Rather, the anodic CAs simply decayed exponentially. In thick films (tens of micrometers), however, a large peak has been seen in the oxidation current.<sup>52</sup> The peak resembles the ESCR peak in anion-transporting materials but is due to a different rate-limiting mechanism. (The cathodic CAs of the thick films, on the other hand, have the same general shape and shoulders found in our thin films.)

The time dependence of the reaction only becomes apparent when the curves are normalized, as in Figure 18b. The oxidation speed increased with increasing anodic voltage, as expected theoretically for the oxidation of a thin film of PPy(DBS).<sup>53</sup> Taking the time at which the current had decayed to 10% of its initial value,  $t_{0.9}$ , as a measure of the speed, one can see that for  $E_{\text{an}} = -0.15$  V and  $t_{0.9} = 2.3$  s, while for  $E_{\text{an}} = +0.4$  V,  $t_{0.9} = 1.8$  s, a difference of  $0.5$  s (Figure 19a). This is a much weaker dependence on the driving voltage than the cathodic current had: recall that (Figure 7) increasing  $E_{\text{ca}}$  from  $-0.7$  to  $-1.4$  produced a drop in  $t_{0.9}$  from  $2.6$  to  $1.1$  s, a difference of  $1.5$  s. This result is consistent with models of ion transport,<sup>32,36,53,54</sup> which show that while reduction is dominated by ion migration in the polymer, and is thus responsive to changes in voltage, ion transport during oxidation is instead dominated by diffusion and is thus only indirectly affected by changes in voltage.

For actuators, these results suggest that it may be possible to speed up the movement during oxidation, by about half a second

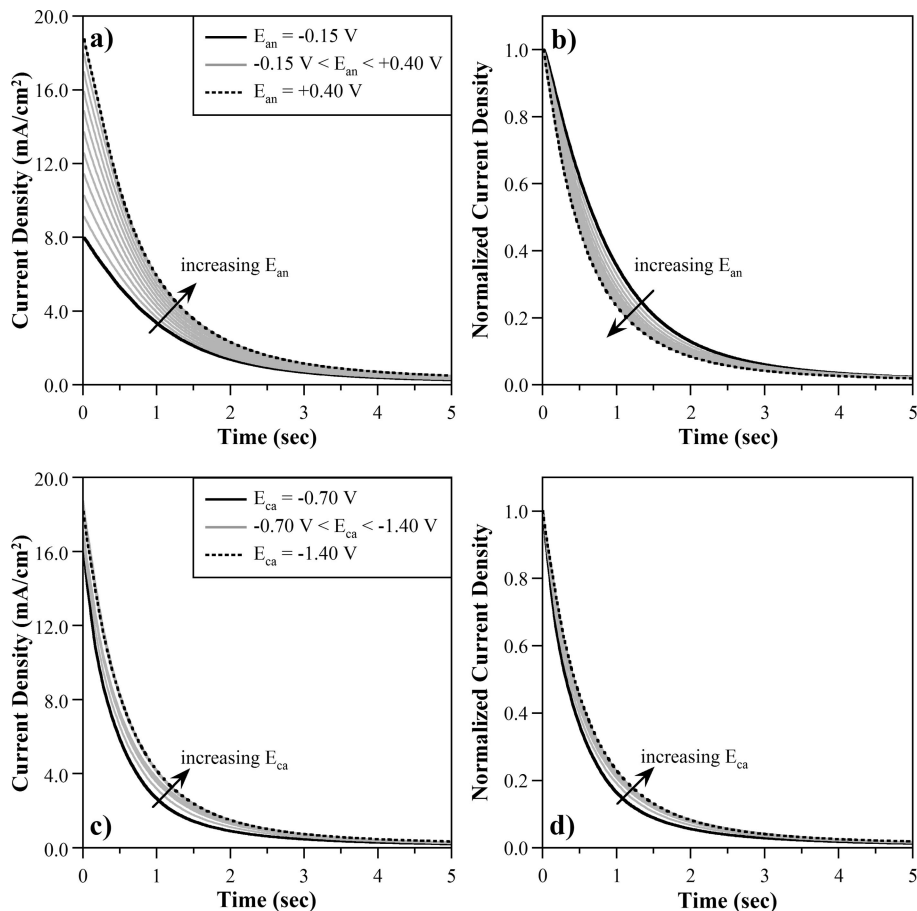


**Figure 18.** (a) Anodic currents upon stepping to different anodic potentials from a fixed cathodic potential ( $-1.40$  V). (b) Same data normalized by the initial current density. (c) Anodic currents upon stepping to a fixed anodic potential ( $+0.40$  V) from different initial cathodic potentials. (d) Normalized versions of the curves in (c).

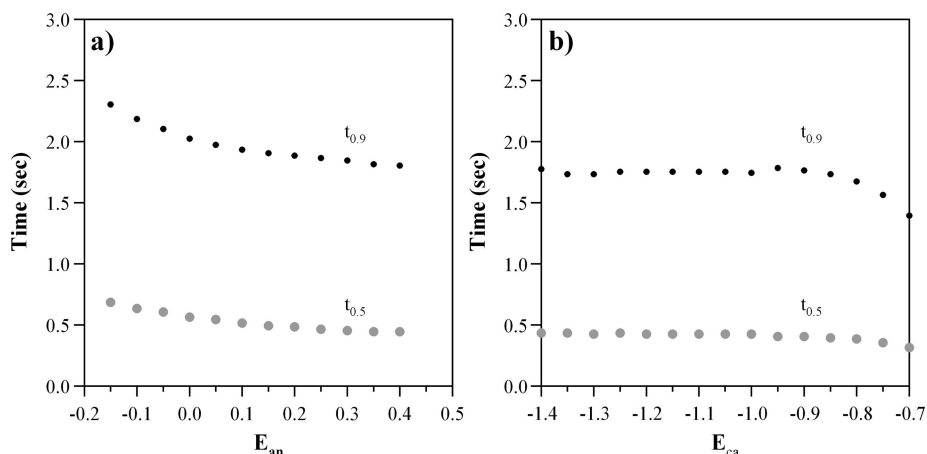


**Figure 19.** Time required for the anodic currents in Figure 18 to fall by 50% and 90% as a function of (a)  $E_{an}$  and (b)  $E_{ca}$ .

at these film thicknesses, by raising the anodic voltage from  $-0.15$  to  $+0.4$  V. However, this assumes that the volume change (associated with Gaussian 1) happens with the same time dependence as the total current shown in Figure 18, but this is not necessarily the case. (Additional work, outside the scope of this paper, would be required to confirm this.) Also, recall that increasing  $E_{an}$  resulted in a longer  $t_{0.9}$  for the subsequent cathodic reaction (by  $0.4$  s over the same range; see Figure 12). Furthermore, this increase in speed comes at a heavy cost of a 90% increase in consumed charge, from  $2.35$  to  $4.5$  mC/cm<sup>2</sup> (obtained by integrating the areas under the CAs; plots of the charge are included in the Supporting Information). Since the *extent* of movement is not

increased by raising the voltage in this anodic range<sup>35,52,55</sup> (in which the polymer is fully oxidized), this speed would come at a cost of a lower efficiency. [Within the potential range of the peaks in Gaussian 1, the movement is a linear function of the charge consumed during Gaussian 1 in PPy (DBS) (see, for examples, Figure 8 and Figure 13 in ref 35). However, in these CAs, the potential limits are beyond that (as shown in Figure 4a) and lie in the region where charge is consumed with no associated movement.] Thus, this method of increasing device speed does not appear to be promising.

Figure 18c shows the effect of stepping to a fixed  $E_{an} = +0.40$  V from a series of increasingly cathodic initial potentials  $E_{ca}$

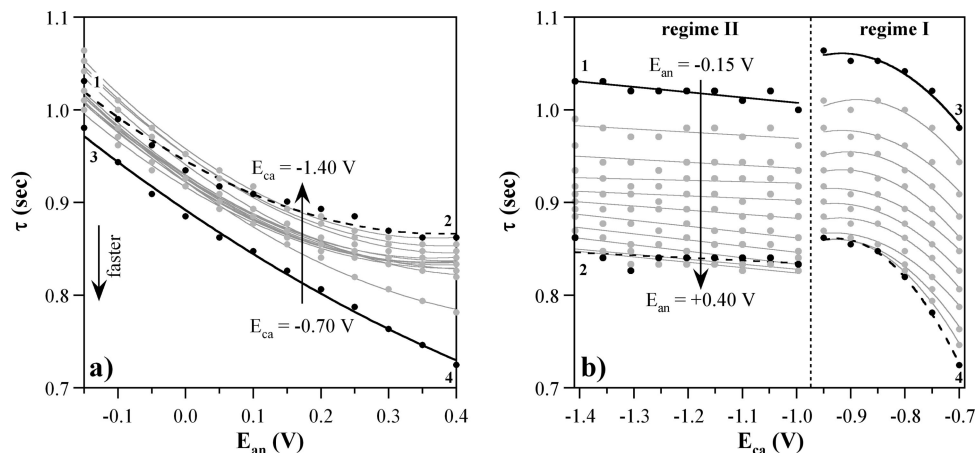


**Figure 20.** (a) Anodic time constant  $\tau$  as a function of  $E_{an}$  for different preapplied cathodic potentials  $E_{ca}$ . Smaller  $\tau$  indicates a faster reaction. (b)  $\tau$  plotted as a function of  $E_{ca}$  for different anodic potentials. The lines are guides for the eye. The labeled points 1–4 indicate how the two plots map one to another.

between  $-0.70$  and  $-1.40$  V. The anodic current increased somewhat as  $E_{ca}$  was raised from  $-0.70$  to  $-1.00$  V, and thereby moved over the tail end of the reduction process (see Figure 4), but the anodic current increased no further thereafter. This result is also consistent with the CVs, in that the PPy reduction is completed by  $-1.00$  V, so that starting at more negative potentials does not lead to greater charge consumed upon oxidation. Further information on charge consumption during anodic stepping is presented in the Supporting Information.

The corresponding normalized curves are shown in Figure 18d. There was a smaller dependence of the speed on  $E_{ca}$  than on  $E_{an}$ , the current decaying somewhat more *slowly* as the preapplied cathodic voltage was increased. This is surprising in light of the ESCR model: as the polymer becomes more reduced, the matrix becomes increasingly open, which one would expect to increase the subsequent oxidation speed. The  $t_{0.5}$  and  $t_{0.9}$  times for the anodic current are shown vs  $E_{ca}$  in Figure 19b. (The two plots match up since the conditions on the right-hand side of (a) are identical to those on the left-hand side of (b):  $E_{ca} = -1.40$  V and  $E_{an} = +0.40$  V.) The reaction speed only slowed down with  $E_{ca}$  up to  $-1.0$  V; beyond that, further increases in the cathodic voltage did not further slow the current decay by this measure. This plateau behavior is consistent with the ESCR model: once the polymer matrix is fully open, ion transport out of the matrix upon subsequent oxidation is unaffected by the initial  $E_{ca}$  and only depends on  $E_{an}$ .

To better understand these time dependences, we now quantify the decay using exponential curve fits.

**3.4.2. Time Constants.** It has consistently been observed (see for example ref 8) that switching of a noncompacted film, as is done during this anodic step in PPy(DBS), gives rise to an exponentially decreasing current. The time constants for the anodic reaction,  $\tau$ , determined by stretched exponential fits as defined in eq 5, are shown for all the data in Figure 20. Smaller values of  $\tau$  correspond to faster switching.

The time constants  $\tau$  are shown vs the anodic potential in Figure 20a. (The curve for  $E_{ca} = -1.40$  V having the black points with the dashed line corresponds to the CA series shown in Figure 18a and the results in Figure 19a.) The faster oxidation reaction rate, due to faster ion transport under higher fields, is reflected in all the curves by the decrease in  $\tau$  with  $E_{an}$ . This decrease was more pronounced when stepping from the partially oxidized state at  $-0.7$  V than when stepping from more negative initial cathodic potentials. The decrease in speed upon raising the cathodic potential from  $-0.7$  to  $-1.0$  is reflected in the rising positions of those curves.

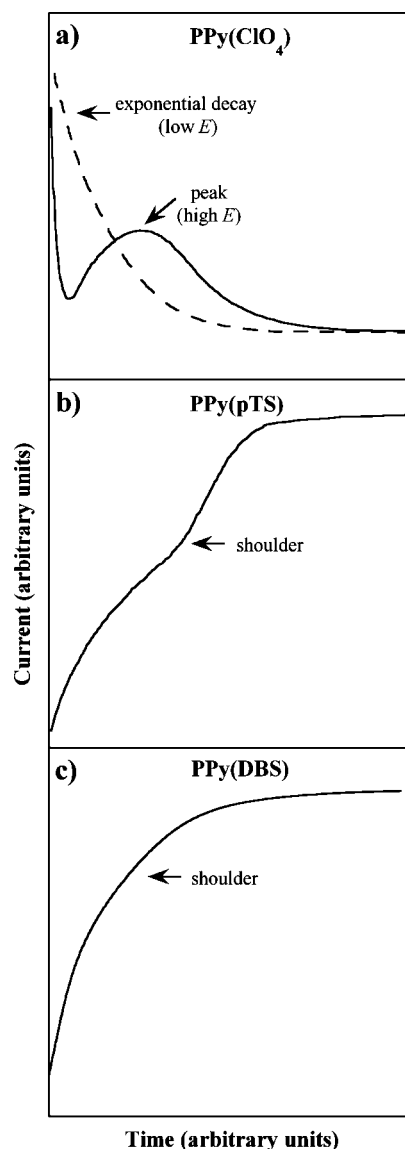


**Figure 21.** Comparison of the shapes of the chronoamperometric peaks in (a) a typical anion-transporting system, PPy( $\text{ClO}_4$ ) cycled in ACN/ $\text{LiClO}_4$ ,<sup>7</sup> and in two cation-transporting systems, (b) PPy(pTS) cycled in PC/ $\text{LiClO}_4$ ,<sup>20</sup> and (c) PPy(DBS) cycled in aqueous NaDBS. Currents and times are not directly comparable because the overpotentials differed, the films varied in thickness, and different electrolytes were used.

TABLE 1: Variables Used in the Paper

variable	meaning
$\tau_r$	time it takes for the relaxation
$\tau_0$	time constant for relaxation
$\Delta H$	molar enthalpy of relaxation
$\Delta H^*$	molar conformational energy consumed in the absence of electric fields
$\Delta H_c$	increment of conformational energy due to the closure of the polymer matrix
$\Delta H_r$	electrochemical energy that contributes to matrix relaxation
$\eta_c$	compaction overpotential (anodic for PPy(DBS))
$\eta_r$	relaxation overpotential (cathodic for PPy(DBS))
$E_c = E_{an}$	applied compaction (= anodic) potential
$E_s$	closure potential: voltage at which the matrix begins to close
$E_r = E_{ca}$	applied relaxation (= cathodic) potential
$E_0$	opening potential: voltage at which reduction begins and the structure starts to open
$z_c$	charge required to compact one mole of polymer segments
$z_r$	charge required to relax one mole of polymer segments
$t$	time
$t_{ESCR}$	position of the ESCR peak in time
$I$	current
$I_0$	current at $t = 0.2$ s
$\tau$	relaxation time of the exponential current decay
$\beta$	stretching coefficient
$\varepsilon$	rms error of the exponential fit to the current decay
$\Gamma_1, \Gamma_2$	regions of the chronoamperometric curve fit by the exponential
$t_{0.5}$	time at which the exponential current has decayed to half-its initial value
$R$	ideal gas constant
$T$	temperature
$Q_{an}$	charge consumed during the anodic step
$Q_{exp}$	charge under the fitted exponential
$Q_{ESCR}$	charge in the subtracted (ESCR) peak
$v$	ion migration velocity

Figure 20b illustrates more clearly how the oxidation kinetics depended on  $E_{ca}$ , the cathodic potential that had been applied just before switching, for all the data. (Again, the black dashed line corresponds to the curves in Figure 18d and closely resembles the results in Figure 19b.) When  $\tau$  is plotted as a function of  $E_{ca}$ , a two-regime behavior can be observed. (This is also seen in the charge, as shown in the Supporting Information.) In regime I,  $\tau$  increases as  $E_{ca}$  becomes more negative, but in regime II, beyond  $-1$  V, there was no further change. In regime I, more cathodic initial potentials increase the reduction level of the polymer. The increase in  $\tau$  might arise because switching from a more reduced state requires more charge to be exchanged (Figures 4 and 18c) (it takes more time to move more charge into and through the polymer at the same  $E_{an}$ ) and/or because of the higher electrical resistance of the more highly reduced state. The effect is greatest for high  $E_{an}$  ( $+0.40$  V), at which  $\tau$  increased 19%, compared to 8% for the lowest  $E_{an}$  ( $-0.15$  V). The increase in  $\tau$  suggests that any benefit to the speed due to matrix opening between  $-0.7$  and  $-1.0$  V (which would decrease  $\tau$  by increasing the mobility and diffusivity of the ions) is more than offset by the increased resistivity. Beyond  $-1.0$  V there is little effect on the subsequent anodic reaction rate from increasing  $E_{ca}$ , since the polymer is already fully reduced and changes no further.

**3.4.3. Summary.** To summarize the results in this section, the anodic currents were well described by simple stretched exponentials regardless of the initial and final voltages. Thus, as expected for a cation-transporting material, there was no

manifestation of conformational relaxation since the matrix was transitioning from an open to a compacted state. The current magnitudes and decay times had a dependence on both initial and final voltages. Higher anodic potentials led to faster reactions (a decrease in response times of up to 50%), as would be expected simply on the basis of ion transport due to diffusion and drift under higher electric fields an open polymer structure. The disadvantage of higher anodic voltages is that they lead to greater charge consumption, which means lower actuator efficiency (same movement but at higher energetic cost). Interestingly, as the initial reduction level of the polymer was increased, the reaction slowed; beyond the fully reduced state, however, there was little further change in speed. Thus, there was no benefit due to starting the anodic step from an even more open initial matrix.

#### 4. Discussion and Conclusions

The presence of the shoulder on the decaying cathodic current, the voltage and holding time dependence of this shoulder, and the absence of a similar shoulder on the decaying anodic current are strong evidence for electrochemically stimulated conformational relaxation in PPy(DBS). The shoulder occurs sooner when the cathodic potential  $E_{ca}$  is increased, with a logarithmic dependence of the peak time on  $E_{ca}$ , consistent with an interpretation that greater cathodic potentials provide more energy for conformational relaxation. The shoulder occurs later as the anodic potential  $E_{an}$  is raised, again with a logarithmic dependence of peak time on  $E_{an}$ , consistent with an interpretation that greater anodic potentials produce greater compaction. Finally, the shoulder occurs later the longer  $E_{an}$  is held prior to the cathodic step, with a power law dependence of the peak time on the holding time, consistent with an interpretation that compaction gradually continues in the anodic state. These matrix effects on ion transport, while not as significant as they are in anion-transporting materials, nevertheless need to be considered in actuator control algorithms, since they give the material a "memory".

As is now clear from examining two cation-transporting systems, PPy(pTS) and PPy(DBS), conformational relaxation plays a much smaller role as a rate-limiting step than it does in anion-transporting polymers (Figure 21). In the latter, the matrix can be compacted to such an extent that switching of every part of the film is delayed until matrix relaxation begins, as evidenced by a single peak in the chronoamperogram (Figure 21a). In the absence of compaction, the chronoamperogram shows only an exponential decay (Figure 21a). On the other hand, in the two cation transporters, even at their most compacted, ESCR affects only a fraction of the charge (20% in PPy(DBS)), and the remaining charge flows freely, as evidenced by the large exponential decay component and the small ESCR peak component. One can therefore conclude that the cation-transporting systems cannot be compacted in aqueous solutions to the same extent as the anion transporters.

The inability to fully compact the cation-transporting polymers is most likely the result of the ions that are always present, in both oxidized and reduced states, and the accompanying water (as illustrated in Figure 1). Prior work on PPy(DBS) has shown that upon the first-ever reduction of the film the out-of-plane volume increases approximately 60% as cations and water are pulled into polymer for the first time<sup>34,35,56</sup> (depending on the cation; these values are for  $\text{Na}^{+57}$ ). Upon reoxidation, however, the film does not contract all the way back to its original thickness: there is a semipermanent increase of  $\sim 25\%$  due to ions and water that remain in the film. Thereafter, the reversible

volume change upon redox cycling is only  $\sim 30\%$ , based on the new oxidized film thickness.

One could make the argument, therefore, that cation-transporting systems may be better suited for actuators with respect to speed and control. Since the switching is less hindered by conformational relaxation, the polymers have less of a memory and should be easier to control. We emphasize, however, that this conclusion is based solely on the chronoamperograms. It would be illuminating to perform analogous voltage stepping experiments with actuators to determine how the CA currents and the movements are correlated. (We also emphasize that it is unclear whether ESCR plays a significant role during actuation in any system when the artificial muscle is performing work or whether other rate-limiting steps come into play under those conditions.) Until analogous studies are done with actuators, measuring the in-plane and out-of-plane volume change as a function of compaction potential and wait time, it is unclear whether the small fraction of charge affected by ESCR is the fraction that is critical for actuation: remember that the amount of charge in Gaussian 1, known from prior work to be associated with actuation and with color change, is of comparable magnitude to the ESCR peak. Further, given that actuation is due to the creation of free volume in the polymer, it would be reasonable to suppose that the ESCR peak current is associated with actuation. The unhindered ion transport presumably represented by the exponential decay component, if it is unassociated with the creation of free volume, may just represent lost actuator efficiency (defined as the fraction of electrical energy converted to mechanical energy) due to ion transport through already-open regions of the polymer matrix. One of the next questions to be answered, therefore, is "what is the role of the charge consumed in the exponential decay?" As pointed out above, this is still unknown. From the point of view of actuator control, answering the question, which cannot be done with the data presented here, of whether the ESCR peak is associated with Gaussian 1 is quite important. If that is the case, then it would explain the time delay in actuation that has been reported between switching the voltage and the commencement of movement. Also, it would demonstrate to what extent movement can be speeded up by applying higher voltages and whether movement is correlated with the position of  $t_{\text{ESCR}}$ .

**Acknowledgment.** We thank Dr. Shawn Walker (previously a graduate student in Dr. Benjamin Shapiro's group) for helping to develop the curve-fitting technique.

**Supporting Information Available:** Details on methodology, data from addition samples, data on charge consumed during chronoamperometry and charge as a function of wait time, and a comparison of conformational energies from various polymers. This material is available free of charge via the Internet at <http://pubs.acs.org>.

## References and Notes

- (1) Lu, W.; Fadeev, A. G.; Qi, B. H.; Smela, E.; Mattes, B. R.; Ding, J.; Spinks, G. M.; Mazurkiewicz, J.; Zhou, D. Z.; Wallace, G. G.; MacFarlane, D. R.; Forsyth, S. A.; Forsyth, M. Use of ionic liquids for pi-conjugated polymer electrochemical devices. *Science* **2002**, *297* (5583), 983–987.
- (2) Jager, E. W. H.; Smela, E.; Inganäs, O. Microfabricating conjugated polymer actuators. *Science* **2000**, *290*, 1540–1545.
- (3) Shimidzu, T.; Ohtani, A.; Iyoda, T.; Honda, K. Charge-controllable polypyrrole/polyelectrolyte composite membranes. Part II. Effect of incorporated anion size on the electrochemical oxidation-reduction process. *J. Electroanal. Chem.* **1987**, *224*, 123–135.
- (4) Wang, X.; Smela, E. Fast switching of conjugated polymer films. *SPIE 13th Annual International Symposium on Smart Structures and Materials*; Bar-Cohen, Y., Ed.; EAPAD: San Diego, CA, Feb 27–Mar 2, 2006; SPIE Vol. 6168.
- (5) Bay, L.; Jacobsen, T.; Skaarup, S.; West, K. Mechanism of actuation in conducting polymers: Osmotic expansion. *J. Phys. Chem. B* **2001**, *105* (36), 8492–8497.
- (6) Otero, T. F.; Grande, H.; Rodriguez, J. Influence of the counterion size on the rate of electrochemical relaxation in polypyrrole. *Synth. Met.* **1996**, *83*, 205.
- (7) Otero, T. F.; Grande, H.; Rodriguez, J. Reinterpretation of polypyrrole electrochemistry after consideration of conformational relaxation processes. *J. Phys. Chem. B* **1997**, *101*, 3688–3697.
- (8) Otero, T. F.; Boyano, I. Comparative study of conducting polymers by the ESCR model. *J. Phys. Chem. B* **2003**, *107*, 6730–6738.
- (9) Otero, T. F.; Boyano, I. Potentiostatic oxidation of polyaniline under conformational relaxation control: Experimental and theoretical study. *J. Phys. Chem. B* **2003**, *107*, 4269–4276.
- (10) Otero, T. F.; Grande, H.; Rodriguez, J. Conformational relaxation during polypyrrole oxidation: From experiment to theory. *Electrochim. Acta* **1996**, *41* (11/12), 1863–1869.
- (11) Otero, T. F.; Grande, H.; Rodriguez, J. Electrochemical oxidation of polypyrrole under conformational relaxation control. Electrochemical relaxation model. *Synth. Met.* **1996**, *76*, 285.
- (12) Otero, T. F.; Grande, H.; Rodriguez, J. A conformational relaxation approach to polypyrrole voltammetry. *Synth. Met.* **1997**, *85*, 1077.
- (13) Grande, H.; Otero, T. F. Conformational movements explain logarithmic relaxation in conducting polymers. *Electrochim. Acta* **1999**, *44*, 1893–1900.
- (14) Odin, C.; Nechtschein, M. Slow relaxation in conducting polymers. *Phys. Rev. Lett.* **1991**, *67* (9), 1114–1117.
- (15) Odin, C.; Nechtschein, M. Slow relaxation in conducting polymers - Influence of the wait potential. *Synth. Met.* **1993**, *55* (2–3), 1287–1292.
- (16) Otero, T. F.; Grande, H. Thermally enhanced conformational relaxation during electrochemical oxidation of polypyrrole. *Electroanal. Chem.* **1996**, *414*, 171.
- (17) Otero, T. F.; Cortes, M. T.; Boyano, I. Molar enthalpy of the polypyrrole electrochemistry. *J. Electroanal. Chem.* **2004**, *562*, 161–165.
- (18) Grande, H.; Otero, T. F.; Cantero, I. Conformational relaxation in conducting polymers: effect of polymer-solvent interactions. *J. Non-Cryst. Solids* **1998**, *235*, 619–622.
- (19) Otero, T. F.; Marquez, M.; Suarez, I. J. Polypyrrole: diffusion coefficients and degradation by overoxidation. *J. Phys. Chem. B* **2004**, *108* (39), 15429–15433.
- (20) Otero, T. F.; Padilla, J. Anodic shrinking and compaction of polypyrrole blend: electrochemical reduction under conformational relaxation kinetic control. *J. Electroanal. Chem.* **2004**, *561*, 167–171.
- (21) Otero, T. F.; Cortés, M. T. Artificial muscles with tactile sensitivity. *Adv. Mater.* **2003**, *15* (4), 279–282.
- (22) Otero, T. F.; Cortes Montanes, M. T. Characterization of triple layers. *SPIE 8th Annual International Symposium on Smart Structures and Materials*; Bar-Cohen, Y., Ed.; EAPAD: Newport Beach, CA, 5–8 March 2001; SPIE Vol. 4329; pp 93–100.
- (23) Otero, T. F.; Cortes, M. T. A sensing muscle. *Sens. Actuators, B* **2003**, *96* (1–2), 152–156.
- (24) Smela, E. Conjugated polymer actuators for biomedical applications. *Adv. Mater.* **2003**, *15* (6), 481–494.
- (25) Jager, E.; Inganäs, W. H. O.; Lundström, I. Microrobots for micrometer-size objects in aqueous media: potential tools for single-cell manipulation. *Science* **2000**, *288*, 2335–2338.
- (26) Bay, L.; West, K.; Sommer-Larsen, P.; Skaarup, S.; Benslimane, M. A conducting polymer artificial muscle with 12% linear strain. *Adv. Mater.* **2003**, *15* (4), 310–313.
- (27) Della Santa, A.; De Rossi, D.; Mazzoldi, A. Characterization and modelling of a conducting polymer muscle-like linear actuator. *Smart Mater. Struct.* **1997**, *6*, 23.
- (28) Smela, E.; Inganäs, O.; Lundström, I. Controlled folding of micrometer-size structures. *Science* **1995**, *268* (23 June), 1735–1738.
- (29) Christophersen, M.; Shapiro, B.; Smela, E. Characterization and modeling of PPy bilayer microactuators. Part I: Curvature. *Sens. Actuators, B* **2006**, *115*, 596–609.
- (30) Smela, E.; Christophersen, M.; Prakash, S. B.; Urdaneta, M.; Dandin, M.; Abshire, P. Integrated cell-based sensors and cell clinics utilizing conjugated polymer actuators. *SPIE 14th Annual International Symposium on Smart Structures and Materials*; Bar-Cohen, Y., Ed.; EAPAD: San Diego, CA, 2007; SPIE Vol. 6524, pp 0G 1–10.
- (31) Wang, X.; Smela, E. Experimental studies of ion transport in PPy(DBS). *J. Phys. Chem. B (accepted)* (**2008**).
- (32) Wang, X.; Shapiro, B.; Smela, E. Development of a model for charge transport in conjugated polymers. *J. Phys. Chem. B* **2008**, accepted.
- (33) Wernet, W.; Monkenbusch, M.; Wegner, G. A new series of conducting polymers with layered structure: Polypyrrole n-alkylsulfates and n-alkylsulfonates. *Makromol. Chem., Rapid Commun.* **1984**, *5*, 157–165.

- (34) Smela, E.; Gadegaard, N. Volume change in polypyrrole studied by atomic force microscopy. *J. Phys. Chem. B* **2001**, *105*, 9395–9405.
- (35) Wang, X.; Smela, E. Color and volume change in PPy(DBS). *J. Phys. Chem. B* **2008**, accepted.
- (36) Wang, X.; Shapiro, B.; Smela, E. Visualizing ion transport in conjugated polymers. *Adv. Mater.* **2004**, *16* (18), 1605–1609.
- (37) Liu, Y.; Gan, Q.; Baig, S.; Smela, E. Improving PPy adhesion by surface roughening. *J. Phys. Chem. C* **2007**, *111* (30), 11329–11338.
- (38) Swager, T. M., personal communication.
- (39) Smela, E.; Kariis, H.; Yang, Z.; Mecklenburg, M.; Liedberg, B. Thiol modified pyrrole monomers: 3. Electrochemistry of 1-(2-thioethyl)-pyrrole and 3-(2-thioethyl)-pyrrole monolayers in propylene carbonate. *Langmuir* **1998**, *14* (11), 2984–2995.
- (40) Smela, E. Thiol modified pyrrole monomers: 4. Electrochemical deposition of polypyrrole over 1-(2-thioethyl)-pyrrole monolayers. *Langmuir* **1998**, *14* (11), 2996–3002.
- (41) Smela, E. Microfabrication of PPy microactuators and other conjugated polymer devices. *J. Micromech. Microeng.* **1999**, *9*, 1–18.
- (42) Diaz, A. F.; Kanazawa, K. K. Polypyrrole: An Electrochemical Approach to Conducting Polymers. In *Extended Linear Chain Compounds*; Miller, J. S., Ed.; Plenum Press: New York, 1983; pp 417–441.
- (43) Salmon, M.; Diaz, A. F.; Logan, A. J.; Krounbi, M.; Bargon, J. Chemical modification of conducting polypyrrole films. *Mol. Cryst. Liq. Cryst.* **1982**, *83* (1), 265–276.
- (44) Skaarup, S.; Bay, L.; Vidanapathirana, K.; Thybo, S.; Tofte, P.; West, K. Simultaneous anion and cation mobility in polypyrrole. *Solid State Ionics* **2003**, *159* (1–2), 143–147.
- (45) Naoi, K.; Oura, Y.; Maeda, M.; Nakamura, S. Electrochemistry of surfactant-doped polypyrrole film(I) -- Formation of columnar structure by electropolymerization. *J. Electrochem. Soc.* **1995**, *142* (2), 417.
- (46) Ariza, M. J.; Otero, T. F. Ionic diffusion across oxidized polypyrrole membranes and during oxidation of the free-standing film. *Colloids Surf., A* **2005**, 226–231.
- (47) Bendler, J. T.; Fontanella, J. J.; Shlesinger, M. F. Anomalous diffusion producing normal relaxation and transport. *J. Phys.: Condens. Matter* **2007**, *19*.
- (48) Wikipedia, “Stretched exponential function”, [http://en.wikipedia.org/wiki/Stretched\\_exponential\\_function](http://en.wikipedia.org/wiki/Stretched_exponential_function), 2008.
- (49) Otero, T. F.; Abadias, R. Poly(3-methylthiophene) oxidation under chemical control. Rate coefficients change with prepolarization potentials of reduction. *J. Electroanal. Chem.* **2007**, *610* (1), 96–101.
- (50) Maw, S.; Smela, E.; Yoshida, K.; Stein, R. B. Effects of monomer and electrolyte concentrations on actuation of PPy(DBS) bilayers. *Synth. Met.* **2005**, *155* (1), 18–26.
- (51) Pei, Q.; Inganäs, O. Electrochemical applications of the bending beam method; a novel way to study ion transport in electroactive polymers. *Solid State Ionics* **1993**, *60*, 161–166.
- (52) Kaneto, K.; Suematsu, H.; Yamato, K. Training effect and fatigue in polypyrrole-based artificial muscles. *Bioinsp. Biomim.* **2008**, *3*, 035005.
- (53) Wang, X.; Shapiro, B.; Smela, E. Model predictions of behavior during reduction of cation-transporting conjugated polymer films. Manuscript in preparation, 2008.
- (54) Wang, X.; Shapiro, B.; Smela, E. Model predictions of behavior during oxidation of cation-transporting conjugated polymer films. Manuscript in preparation, 2008.
- (55) Shimoda, S.; Smela, E. The effect of pH on polymerization and volume change in PPy(DBS). *Electrochim. Acta* **1998**, *44*, 219–238.
- (56) Smela, E.; Gadegaard, N. Surprising volume change in PPy(DBS): an atomic force microscopy study. *Adv. Mater.* **1999**, *11* (11), 953–957.
- (57) Wang, X.; Smela, E. Cycling conjugated polymers with different cations. *SPIE 13th Annual International Symposium on Smart Structures and Materials*; Bar-Cohen, Y., Ed.; EAPAD: San Diego, CA, Feb 27–Mar 2, 2006; SPIE Vol. 6168.

JP8058245

# Supporting Information for Chronoamperometric Study of Conformational Relaxation in PPy(DBS)

B. Jason West, Toribio F. Otero, Benjamin Shapiro, and Elisabeth Smela

## 1 METHODOLOGY

### 1.1 Effect of the Working Electrode Surface

The effect of the working electrode surface must be considered in this type of study, since it is thought to strongly influence the kinetics of relaxation [1]. The ESCR model was developed based on experimental data obtained from PPy films of very uniform thickness deposited by square potential waves on mirror polished Pt. In those (anion-transporting) systems, nucleation was observed in the form of expanding cylinders that coalesced over time (visible via the electrochromism of these polymers). The ESCR model thus included the effects of nucleation and coalescence. This is in contrast to the uniform color changes during switching in our study, which employed as substrates thermally evaporated Au on highly polished Si (see Figure 1-SI): no nucleation occurred (or, conversely, nucleation occurred in so many places at once that it could not be observed). So, while our results agree with the ESCR model, it should be noted that future work should adapt the model to include uniform front propagation (i.e., one flat nucleus). Future models should also include the role of drift on ion transport.

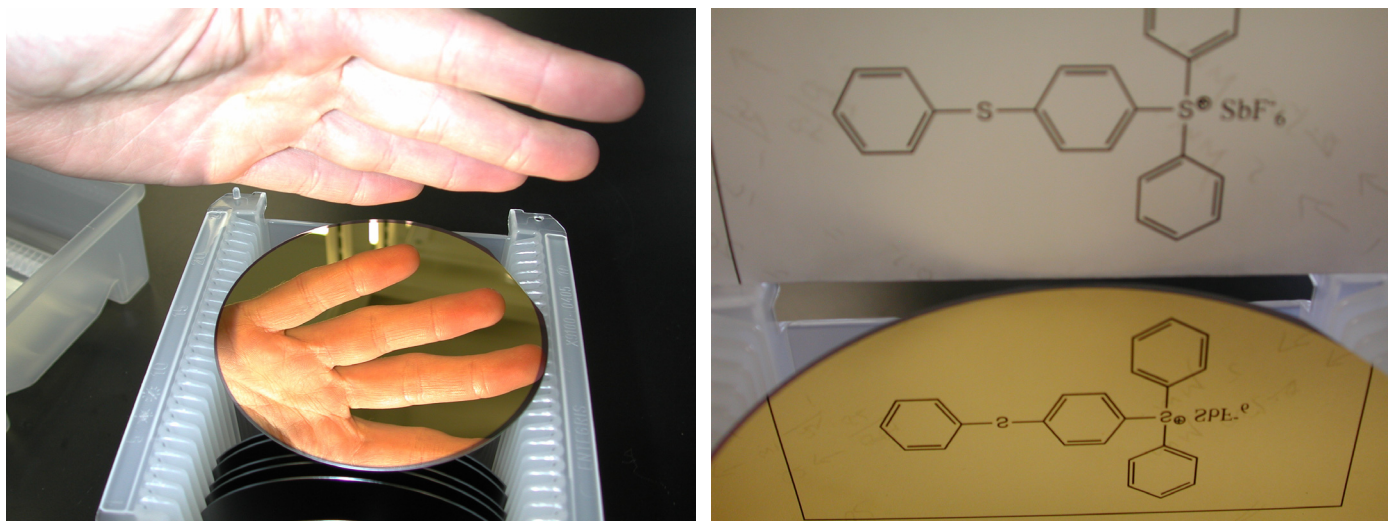


**Figure 1-SI.** Photographs of the mirror-like surface of a representative Au-covered, oxidized Si wafer that was used in the study.

### 1.2 Effect of PPy Thickness

The PPy thickness was also of importance in determining the results of this study. Since the films were fairly thick (5000 Å), ion transport occurred simultaneously both in the in-plane and the out-of-

plane directions, again observed via the electrochromism of the films. (This is typical for PPy(DBS).) This complicates data analysis, since both ion mobility and conformational relaxation could be different in the two directions. Future work involving films of varying thickness and area showing how the cathodic current shoulder evolves would help to explain the role that conformational relaxation plays in ion transport in the two directions.

### 1.3 Exponential Curve Fitting

The use of exponential functions to fit the CA data, rather than a  $t^{-1/2}$  relationship as is usually used in electrochemistry (the Cottrell equation), may be surprising to some readers. It is important to recall that the Cottrell expression is based on the diffusion of species in a liquid electrolyte to the surface of a solid electrode; it does not take into account migration (movement of charge under electric fields), nor does it take into account species moving through a polymer matrix.

The stretched exponential function has been used to empirically describe a range of physical properties in complex systems such as polymers and glasses [2-4]. It can also be used to fit a distribution of diffusion times in swelling/shrinking polymers. The distribution of times is thought to arise from local variations in the diffusion coefficients within the polymer due to local differences in oxidation level, swelling, crosslinking, chain stiffness, etc. Just as defects and crosslinking produce a distribution of oxidation and reduction potentials, and thus broad peaks in the cyclic voltammograms compared to those obtained for electrochemical reactions at liquid/solid interfaces, these parameters would be expected to affect the scattering of ions, and thereby the diffusion coefficient.

The movement of ions through a dense polymer electrode whose properties (oxidation level, volume, chain stiffness, solvation) are changing simultaneously with the arrival or departure of those very ions, makes this redox a complex process. It is further complicated by the fact that migration cannot be neglected [5,6]. Furthermore, as shown by these and prior papers on ESCR processes, the rate-limiting step may not be diffusion at all, but may be changes in chain conformation. Therefore, one should not expect the Cottrell equation to apply.

## 2 CYCLIC VOLTAMMETRY

Figure 2-S1a shows cyclic voltammograms taken periodically throughout a CA series on one sample, and Figure 2-S1b shows single scans from each of the three samples used in the study. As explained in section 2.1.3 of the main text, these scans were recorded in order to ascertain the state of the films following each set of CA steps. Figure 2-S1a shows that there was relatively little change between cycles, which means that the samples did not significantly delaminate or degrade during the course of the study. Figure 2-S1b shows that the reduction and oxidation peaks occurred at the same potentials for each sample used in the study, showing that the results from each sample are comparable. (The variation in charge from sample to sample is due variation in the width of the samples (they varied by  $\sim 1$  mm) and the immersed depth of the samples (which also varied by  $\sim 1$  mm).)

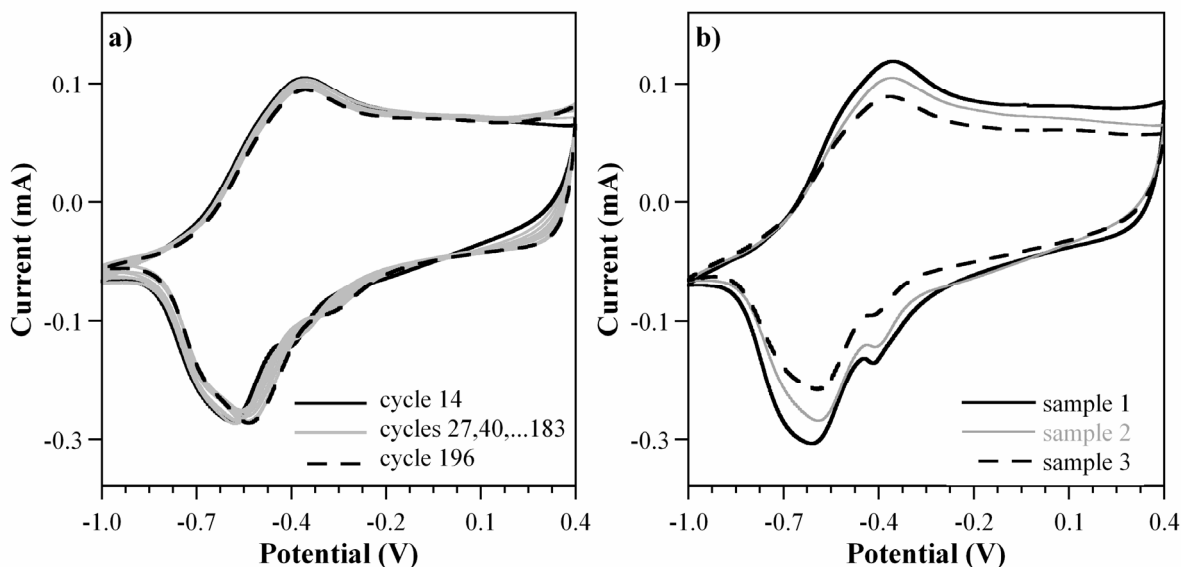


Figure 2-SI. Cyclic voltammograms of a) 13-CA-cycle increments up to 196 cycles on one sample, and b) single cycles from all three samples used in the study.

### 3 CATHODIC CURRENTS DURING CHRONOAMPEROMETRY

#### 3.1 Role of Cathodic Potential

The evolution of the cathodic CAs with increasingly cathodic potential  $E_{ca}$ , from -0.7 to -1.4 V, is shown in Figure 3-SIa, and corresponds to data in Figure 6 in the main text. The two-regime behavior was observed on all three samples. Exponential curve fits and the resulting ESCR peaks are shown in Figure 3a) and b).

Figure 4-SI (also corresponding to Figure 6 in the main text) shows cathodic curve fits for a single pre-applied  $E_{an}$  (+0.40 V), stepping to three successively higher cathodic potentials  $E_{ca}$ . These fits are shown primarily to illustrate the point at which  $\Gamma_1$ , (recall that  $\Gamma_1$  and  $\Gamma_2$  are the regions of the CA curves in which the curve fitting error was calculated) shrank to zero. This point was estimated to be -1.05 V; please note that at -1.00 V, there is still a small delay on the ESCR peak, corresponding to a small region of the CA curve which was fit with the exponential.

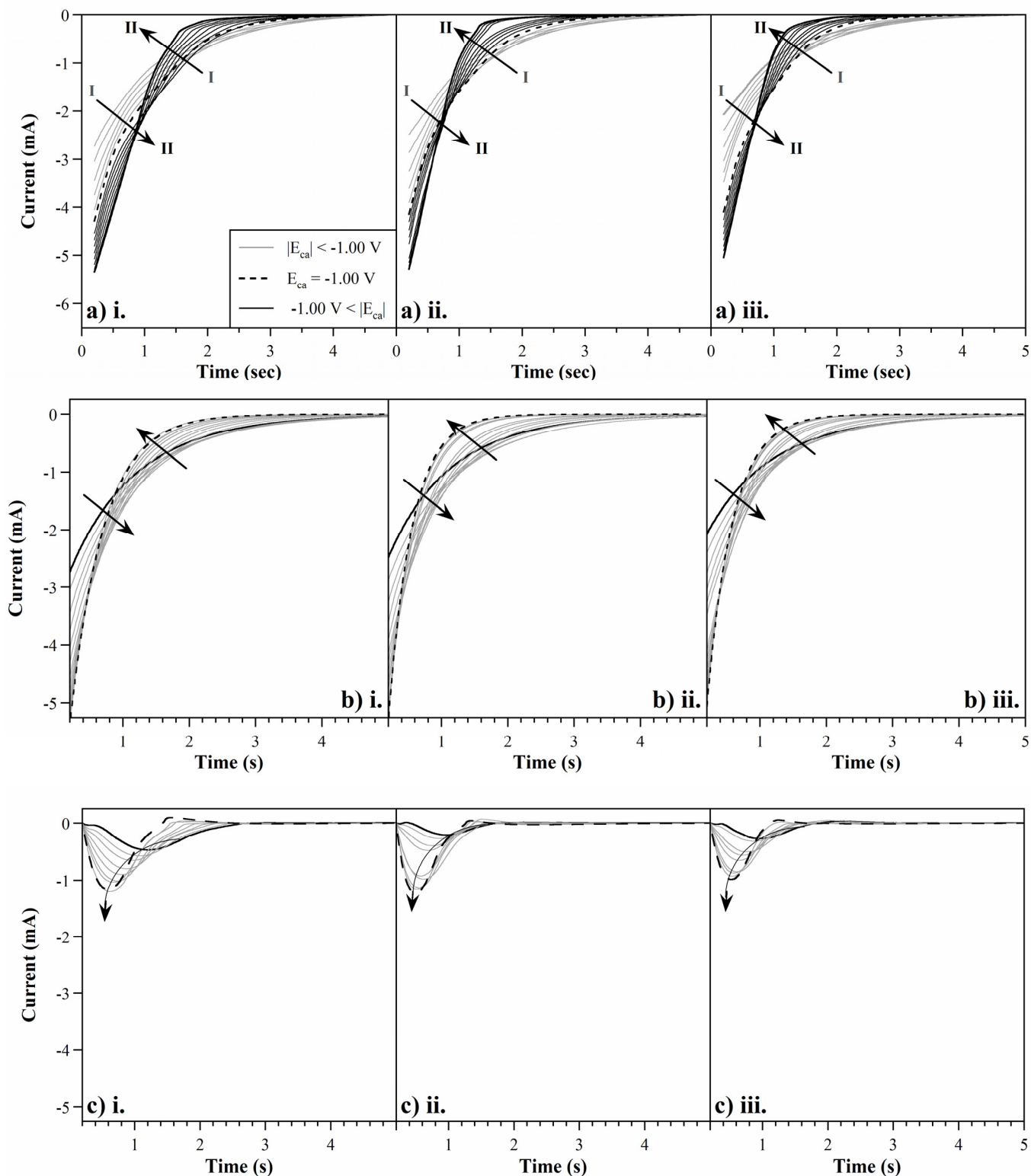


**Figure 3-SI. a) Total cathodic currents and b) exponential and c) ESCR components of cathodic curve fits for increasingly cathodic initial potentials from an initial  $E_{an}=+0.40$ V. Data from the three studied samples are denoted by roman numerals.**

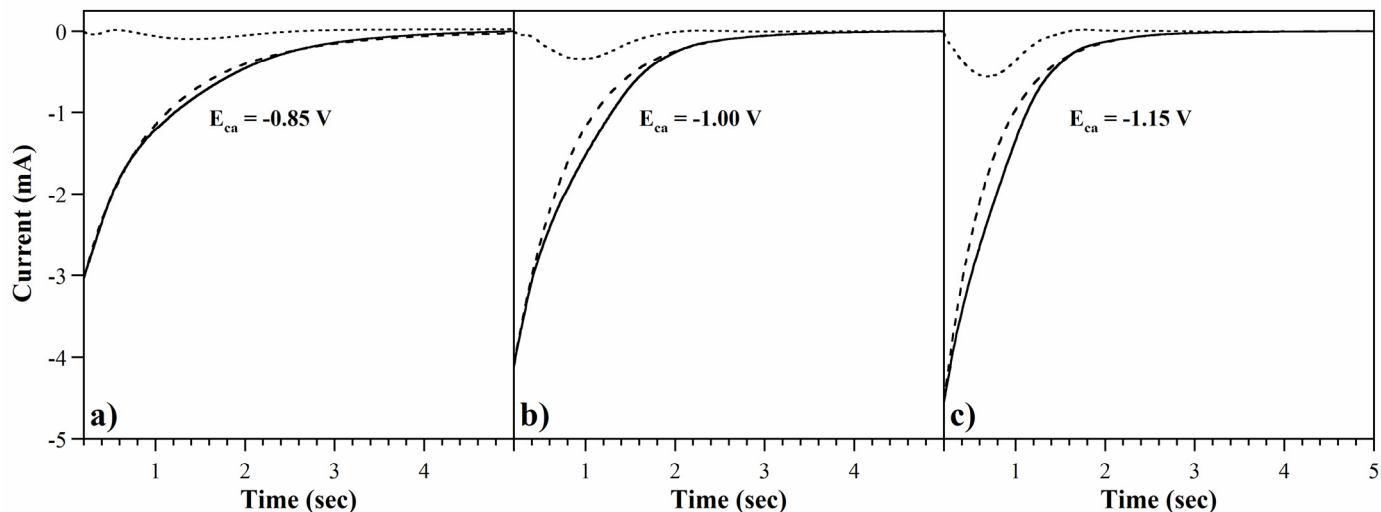


**Figure 4-SI.** a) CA data (solid curves), exponential fits (dashed lines), and subtracted (ESCR) components (dotted lines) for  $E_{ca} = -0.85$  V, stepping from  $E_{an} = +0.40$  V. b) Fitted curves for  $E_{ca} = -1.00$  V. c) Fitted curves for  $E_{ca} = -1.15$  V.

### 3.1.1 Time Dependence: Exponential Curve

In Figure 5-SI (corresponding to Figure 10 in the main text), the natural log of the cathodic exponential time constant,  $\ln(\tau_{exp})$ , is plotted as a function of  $E_{ca}$  for the three samples. Small differences were observed, but the trend was the same for all of the samples.

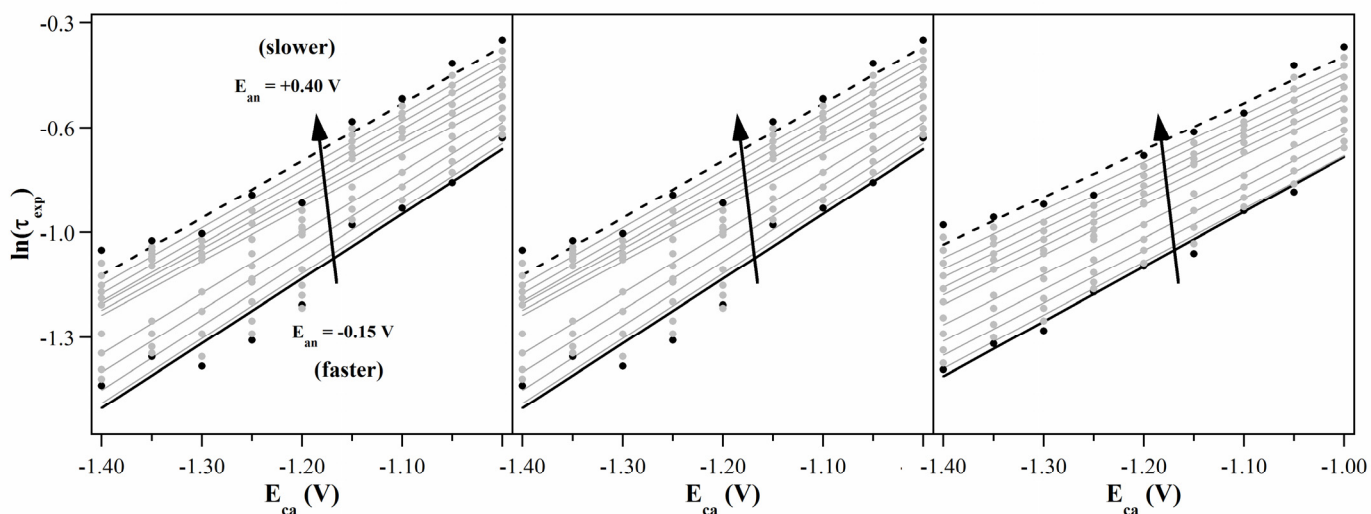


**Figure 5-SI.** Natural logarithm of the time constants for the exponential curve fits to the tails of the cathodic CAs, plotted as a function of cathodic potential upon stepping from different pre-applied anodic potentials (the lines are a guide to the eye).

### 3.1.2 Time Dependence: ESCR Peak

Figure 6-SI (which corresponds to Figure 11 in the main text) shows the ESCR peak position in time,  $\tau_{ESCR}$ , as a function of  $E_{ca}$  for the three samples.

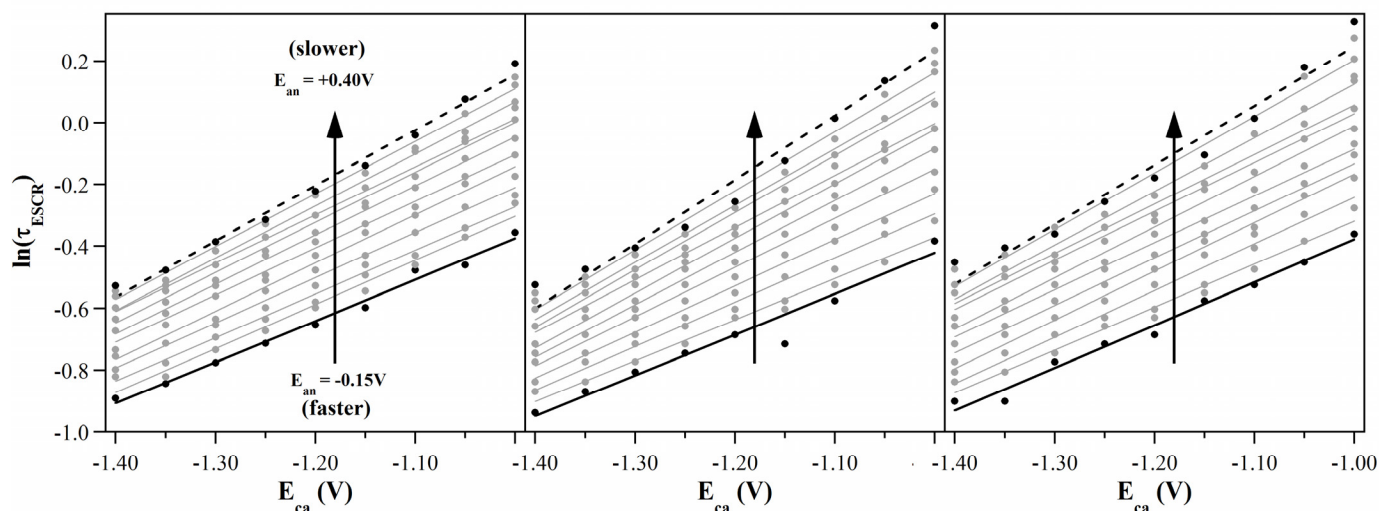


**Figure 6-SI.** Natural logarithm of the time constants for the subtracted (ESCR) curves, plotted as a function of cathodic potential upon stepping from different pre-applied anodic potentials (lines).

### 3.1.3 Charge

The consumed cathodic charge,  $Q_{ca}$ , the charge in the fitted exponential,  $Q_{exp}$ , and the charge in the subtracted peak,  $Q_{ESCR}$ , are shown as a function of  $E_{ca}$  in Figure 7-SI (the consumed cathodic charge corresponds to Figure 8 in the main text).  $Q_{exp}$  decreases linearly with increasingly cathodic potentials for the entire range of anodic potentials. As expected,  $Q_{ESCR}$  experiences a corresponding increase with increasingly cathodic potentials to compensate for the leftover charge\*. The increase of  $Q_{ESCR}$  and the decrease of  $Q_{exp}$  with increasing cathodic potential are consistent with the ESCR model, assuming that the peak is related to conformational relaxation. Additionally,  $Q_{ESCR}$  and  $Q_{exp}$  correspond well with the charge densities and proportions of the two Gaussian peaks in the CVs (paper Figure 4b).

Note that the x-axes in a) extend to -0.7 V, but only to -1.0 V in b) and c), because only curve fits at  $E_{ca}$  more cathodic than -1.0 V were considered. The charges ( $Q_{ca}$  vs.  $Q_{exp}+Q_{ESCR}$ ) don't match up because the curve fitting was only done past 0.2 seconds, so the fitted charges only include those data.

\* Keep in mind that at this point in the data analysis, the original data have been: 1) corrected for baseline current at 5 s, 2) corrected for capacitive current below 0.2 s, 3) partially fit with exponential curves, and 4) the two components of the fitted curves have been integrated to obtain the charge in Figure 7-SI. With this many levels of processing, we do not intend to make exact statements about the data, especially with the ESCR peaks, which contain ~20% of the charge of the exponential peaks, and are thus ~5x more susceptible to noise in data processing. Rather, we present these data to show *general* trends that are nonetheless consistent across all three data sets and consistent with the ESCR model.

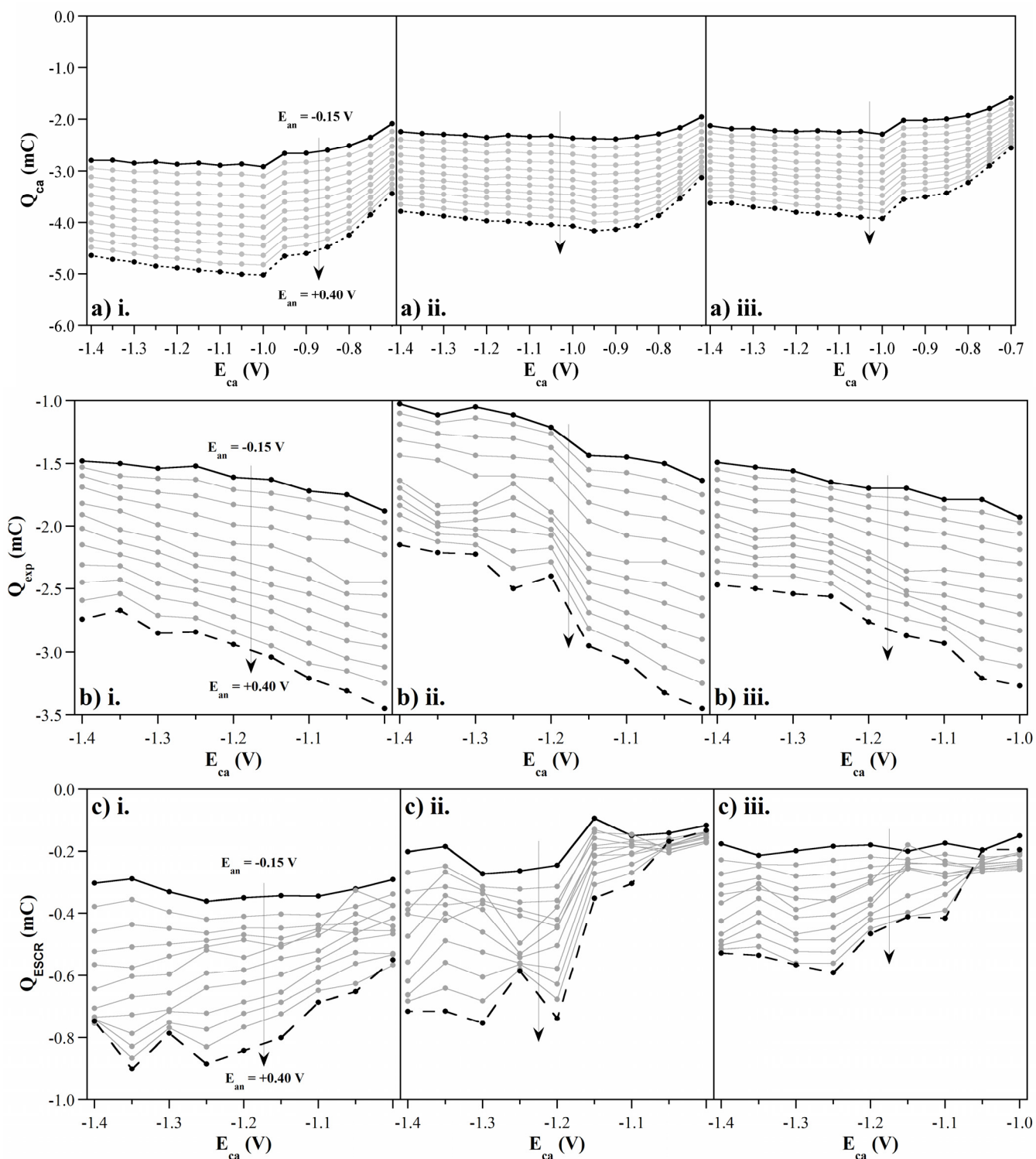


**Figure 7-SI.** Cathodic charge consumed during steps to various cathodic potentials, calculated from a) the original experimental data, b) the exponential fits, and c) the subtracted peak components as a function of  $E_{ca}$  for a series of initial  $E_{an}$ . Data from the three studied samples are denoted by roman numerals.

### 3.2 Role of Anodic Potential

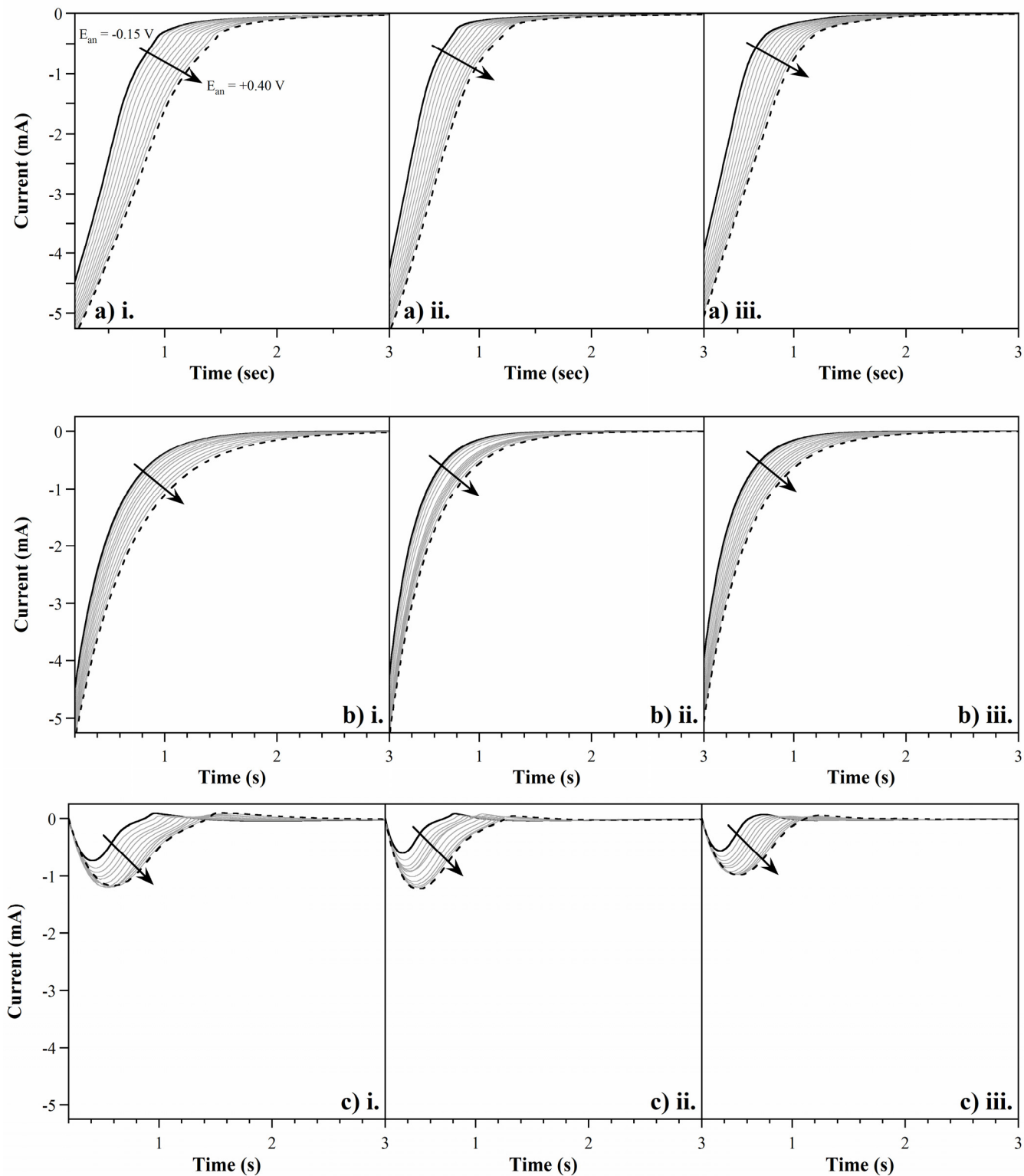
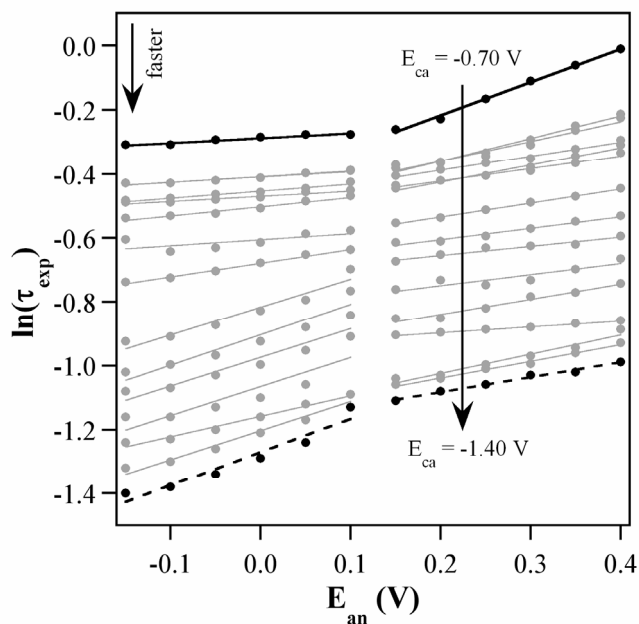


Figure 8-SI. a) Cathodic currents , b) exponential and c) ESCR components of cathodic curve fits for increasingly anodic initial potentials from an initial  $E_{ca} = -1.40$  V. Data from the three studied samples are denoted by roman numerals.

Figure 8-SI shows cathodic CAs (row a), exponential curve fits (row b), and ESCR curves (row c) for a single  $E_{ca}$  (-1.40 V) vs.  $E_{an}$ . This plot corresponds to Figures 12 and 13 in the main text.

### 3.2.1 Time Dependence: Exponential Curve

The logs of the time constants obtained from the exponential fits are plotted as a function of  $E_{an}$  in Figure 9-SI. For all  $E_{ca}$ , the times increased slightly with anodic potential,  $E_{an}$ . The reasons for this are not yet clear, since the exponential current during reduction is presumably due to unimpeded ion transport in an open matrix (only the ESCR peak is expected to reflect compaction). As  $E_{ca}$  was increased, the lines moved downward, reflecting the faster cathodic response under more negative voltages that was detailed in the paper (Figure 10).



**Figure 9-SI. Cathodic exponential time constants as a function of the pre-applied anodic potential upon stepping to different cathodic potentials.**

The increase in  $\tau_{exp}$  occurred even for  $E_{ca} = -0.7, -0.75, \text{ and } -0.80$ , for which there was no ESCR peak. In addition, the increase was seen in all three data sets (shown in Figure 10-SI). This is therefore a real effect. Between  $E_{an} = -0.15 \text{ and } +0.1 \text{ V}$ , there was a change in slope at approximately  $E_{ca} = -1.00 \text{ V}$ , corresponding to when the polymer becomes fully reduced and the subtracted curves become significant compared to the noise. For higher  $E_{an}$ , the slopes remained essentially constant.

For  $E_{ca} = -0.7, -0.75, \text{ and } -0.80$ , the  $\tau_{exp}$  were obtained by fitting the entire CA curve, since there was no ESCR peak at those low cathodic potentials; confidence in these values can therefore be high. One can also have confidence in the time constants for  $E_{ca} = -0.85 \text{ through } -1.10 \text{ V}$ , for which the curve fits were able to use some portion of the beginning of the curve ( $\Gamma_1 \neq 0$ ). The  $\tau_{exp}$  for  $E_{ca}$  more negative than  $-1.10 \text{ V}$ , obtained from curve fits for which  $\Gamma_1 = 0$ , were consistent with the other lines, so it is likely that these results are also reliable.

As mentioned above, if the exponential is due to transport of ions in an open matrix, one would not expect a dependence on  $E_{an}$ . One possibility is that starting from higher anodic potentials results in slower switching since it requires more charge to be exchanged (see the CV in the paper, Figure 4), or that this increment of charge goes to different types of sites in the polymer, or to other reactions. Resolving this question would require further studies outside the scope of this paper.

Figure 10-SI compares the dependence of  $\ln(\tau_{exp})$  on  $E_{an}$  for all three data sets. Results were again consistent for the three samples.

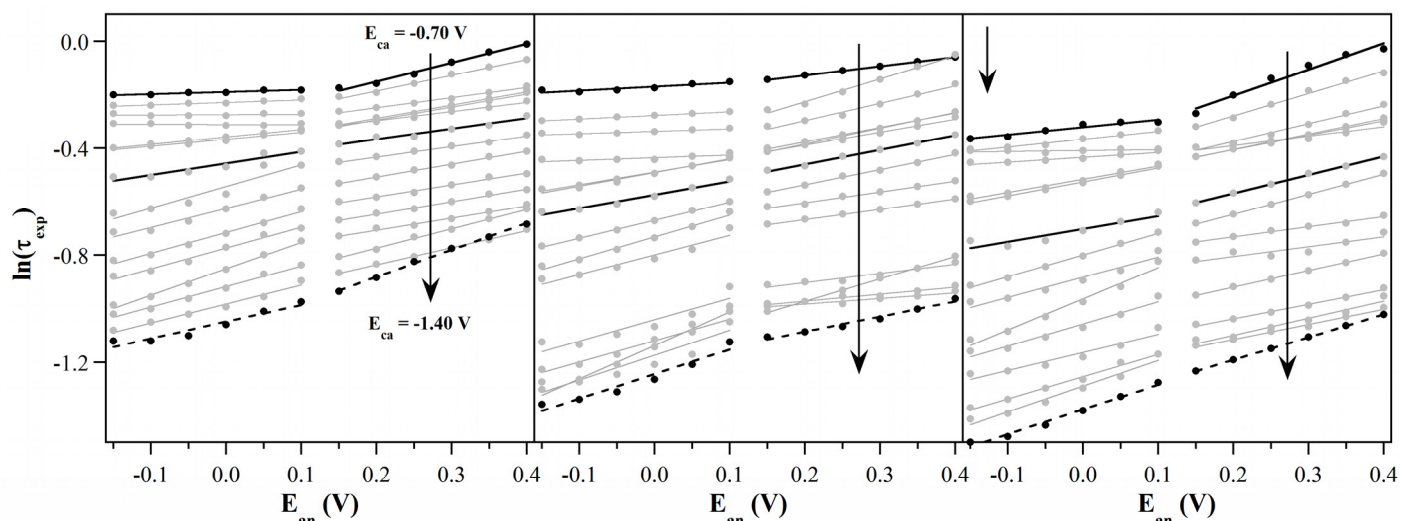


**Figure 10-SI. Cathodic exponential time constants as a function of the pre-applied anodic potential upon stepping to different cathodic potentials.**

### 3.2.2 Time Dependence: ESCR Peak

ESCR peak times  $\tau_{ESCR}$  are plotted vs.  $E_{an}$  in Figure 11-SI (corresponding to Figure 14 in the main text). Results were consistent across all samples.

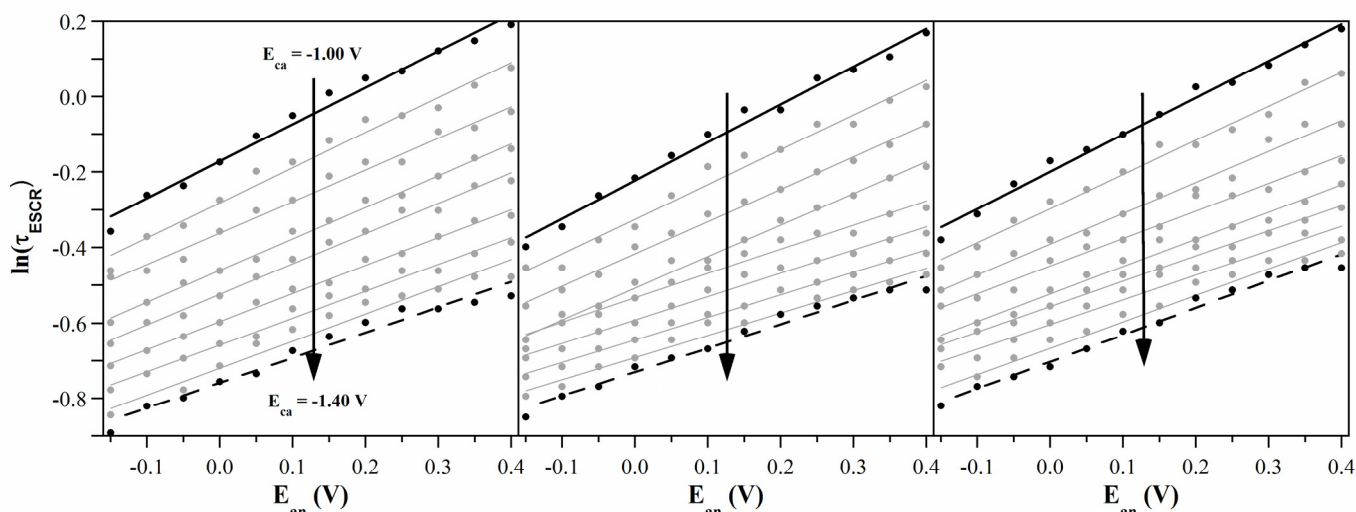


**Figure 11-SI. Natural log of the ESCR peak time as a function of pre-applied anodic potential.**

### 3.2.3 Charge

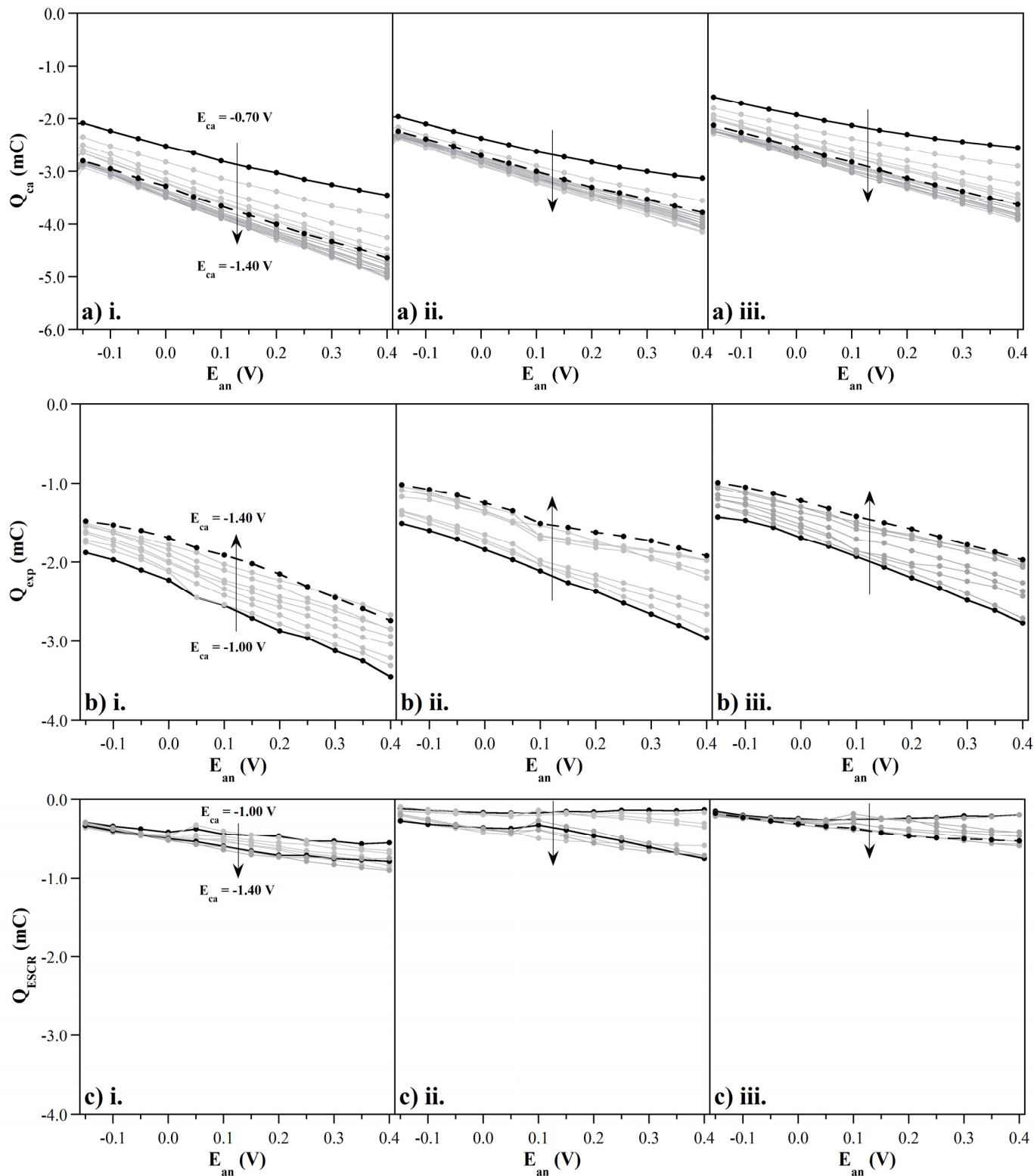


**Figure 12-SI.** Cathodic charge consumed during steps to different anodic potentials, calculated from a) the original experimental data, b) the exponential fits, and c) the subtracted peak components as a function of  $E_{an}$  for a series of initial  $E_{ca}$  (-1.40 V). Data from the three studied samples are denoted by roman numerals.

Analogously to Figure 7-SI, which examined the consumed cathodic charge as a function of cathodic potential, Figure 12-SI shows the cathodic charge, exponential charge, and ESCR peak charge as a function of the applied anodic potential. There is no corresponding plot in the main text. Consistency was observed for all samples.

### 3.3 Role of Wait Time

Figure 16 in the paper showed that the total charge increased with the holding time. Figure 13-SI shows that the charge increased logarithmically with holding time, just as the peak position did.\*

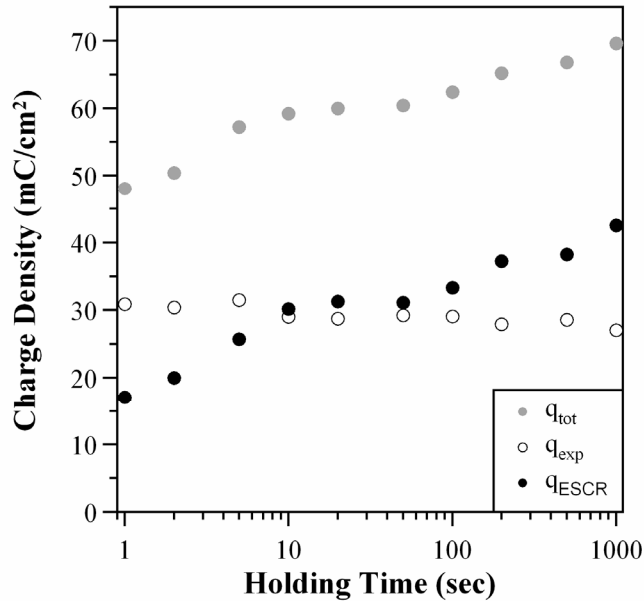
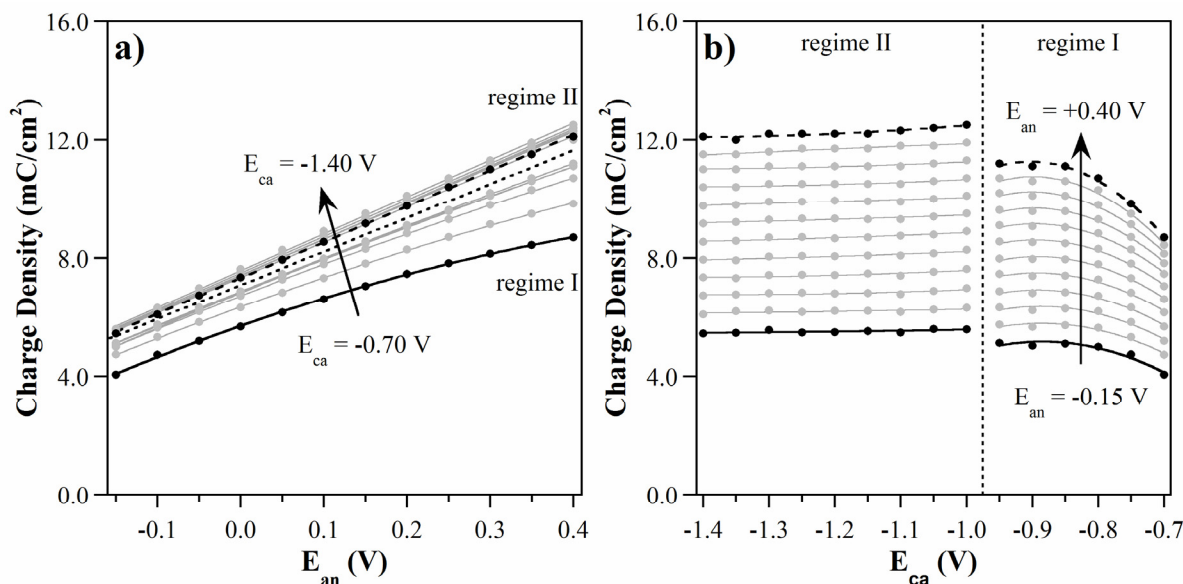


Figure 13-SI. Absolute magnitude of the cathodic charge densities as a function of holding time: total (gray), exponential (empty), and ESCR (black) charge.

\* Given the fixed exponential fit for all the curves, when the total charge  $q_{tot}$  was split into exponential and ESCR components, only the ESCR charge  $q_{ESCR}$  could increase with holding time. The small decrease in  $q_{exp}$  with holding time is due to the fact that the charge integration started at  $t = 0.2$  rather than  $t = 0$  seconds.

#### 4 ANODIC CHARGE CONSUMED DURING CHRONOAMPEROMETRY



**Figure 14-SI. Anodic charge as a function of a) anodic potential for different initial cathodic potentials and b) cathodic potential for different anodic potentials. The measured values are indicated by points; the lines are a guide to the eye. The dotted line separates the curves in regimes I and II.**

The charge consumed during the anodic step,  $Q_{an}$ , was calculated by integrating the area under the current-corrected CA curve between 0 and 5 seconds. Figure 14-SI shows  $Q_{an}$  as a function of  $E_{an}$  and  $E_{ca}$ . When stepping from cathodic potentials that lie below the peak for the reduction process in the PPy(DBS), i.e.,  $E_{ca} \leq -1$  V (upper curves in Figure 14-SIa), the charge increased essentially linearly with  $E_{an}$ , consistent with the constant pseudo-capacitive current in the CVs above -0.15 V. Furthermore, the curves overlay each other. This means that increasing the cathodic potential does not change the amount of charge consumed by the subsequent oxidation. This range of potentials will be referred to as “regime II”.

When stepping from less cathodic potentials,  $E_{ca} > -1$  V (lower curves in Figure 14-SIa), the charge increased less rapidly with  $E_{an}$ , and the charge depended on  $E_{ca}$ . This range of potentials will be called “regime I”. In regime I, the reduction level of the polymer depends on  $E_{ca}$ , whereas in regime II the polymer is fully reduced, and cannot be further reduced by increasing  $E_{ca}$ . The same data are plotted as a function of  $E_{ca}$  in Figure 14-SIb, where the two regimes are evident. There was a discontinuity between -0.95 and -1.00 in all the data, the reason for which is unclear.

## 5 CONFORMATIONAL ENERGIES $z_c$ AND $z_r$ IN VARIOUS POLYMERS

The values of the conformational energies  $z_c$  and  $z_r$  found in this work are compared with the values reported for other systems in Table I-SI and Figure 15-SI. In anion-transporting polypyrroles, the values of  $z_c$  and  $z_r$  are generally larger than those in PPy(DBS). However, it is important to note that these numbers cannot be directly compared because the film thicknesses were different, and film thickness affects these values since the molecular structure changes as a function of polymerization time. In addition, in order to use these values in a comparative way, a material reference is required, i.e. the charge consumed per unit of PPy mass during a voltammetric step to the same anodic over-potential.

**Table I-SI. Values of the conformational energies in various systems.**

Polymer	Solvent	Salt	$z_c$ (kC/mol)	$z_r$ (kC/mol)	$\Delta H^*$ (kJ/mol)	$\Delta H$ (kJ/mol)	Reference
<b>Cation-Transporting Polypyrroles</b>							
PPy(DBS)	water	NaDBS	1.5–2.6	2.8-4.5			this work
PPy(pTS)	PC	LiClO <sub>4</sub>	2.4				[7]
<b>Anion-Transporting Polypyrroles</b>							
PPy	ACN	LiClO <sub>4</sub>	4.2	7.4			[8]
PPy	ACN	LiClO <sub>4</sub>	3.5			28	[9]
PPy	ACN	LiClO <sub>4</sub>	5.6	2.7			[10]
PPy	PC	LiF, LiCl, LiI, LiBr	2.2				[11]
PPy	PC	LiClO <sub>4</sub>	3.2-5.2 <sup>††</sup>				[12]
PPy	PC	LiClO <sub>4</sub>	2.5	6.0	21.3		[13]
PPy	PC	LiClO <sub>4</sub>	4.6	4.4-7.7 <sup>†</sup>			[14]
PPy	PC	LiClO <sub>4</sub>	4.4	5.4	28		[15]
PPy <sub>zdc/n</sub>	PC	LiClO <sub>4</sub>	4.1	6.0			[10]
PPy	sulfolane	LiClO <sub>4</sub>	3.1	9.0			[10]
PPy	acetone	LiClO <sub>4</sub>	3.6	8.0			[10]
PPy	DMSO	LiClO <sub>4</sub>	4.5	4.7			[10]
PPy	water	LiClO <sub>4</sub>				27	[16]
<b>Anion-Transporting Polyaniline</b>							
PANI	ACN	LiClO <sub>4</sub>	5.5	3.5-9.6 <sup>†</sup> from text 4.7-11.7 <sup>†</sup> from graph	14		[17]
PANI	ACN	LiClO <sub>4</sub>	5.5			14	[9]
<b>Different Anion-Transporting Polymers</b>							
poly(1-methyl pyrrole)	ACN	LiClO <sub>4</sub>	4.4			17	[9]
poly(methyl-aniline)	ACN	LiClO <sub>4</sub>	6.9			10	[9]
poly(thiophene)	ACN	LiClO <sub>4</sub>	2.7			24	[9]
poly(3-methylthiophene)	ACN	LiClO <sub>4</sub>	3.5			16	[9]

<sup>†</sup> The coefficient  $z_r$  depends on the pre-applied compaction potential.

<sup>††</sup> The coefficient  $z_c$  depends on the time spent in the compacted state.

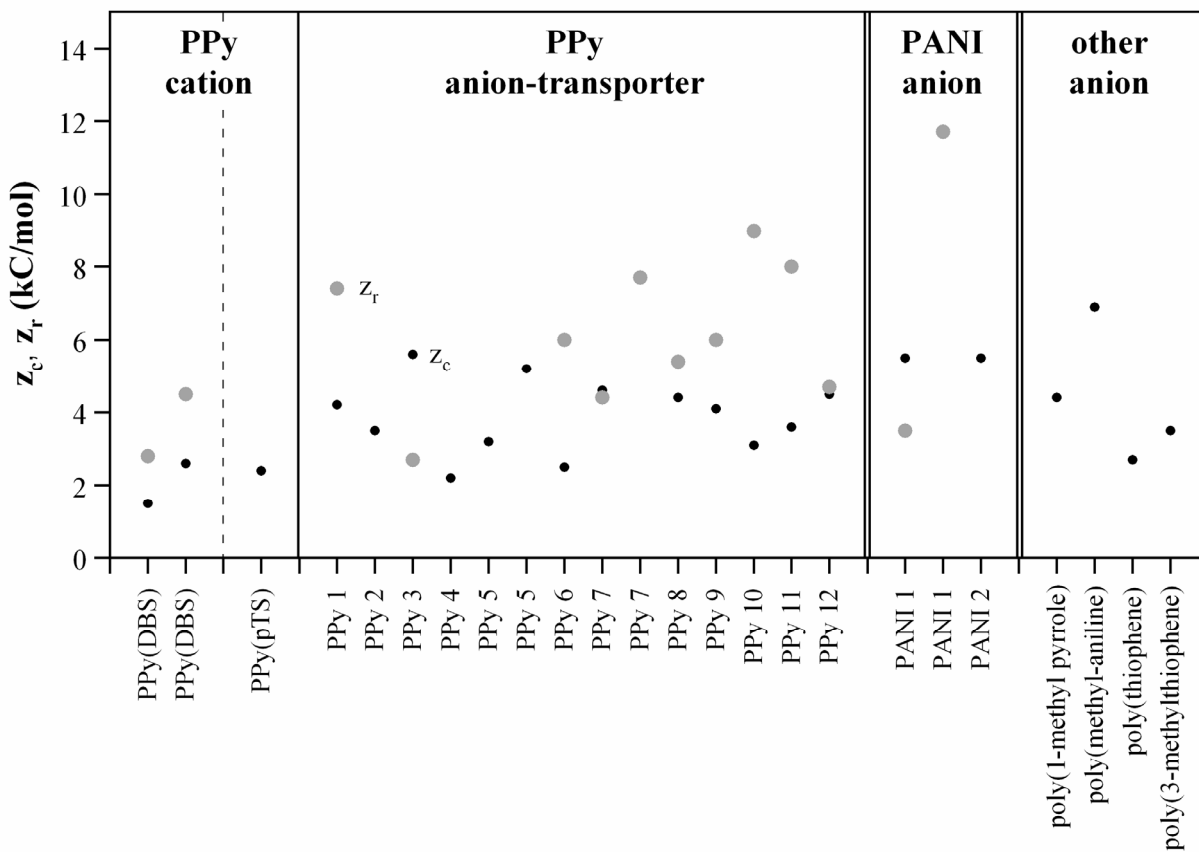


**Figure 15-SI.** Values of the conformational energies  $z_c$  (black dots) and  $z_r$  (gray dots) in various systems. .

## REFERENCES

1. T. F. Otero, H. Grande, and J. Rodriguez, "Reinterpretation of polypyrrole electrochemistry after consideration of conformational relaxation processes," *J. Phys. Chem. B*, 101, 3688-3697 (1997).
2. R. Kohlrausch, "Theorie des elektrischen rückstandes in der leidner flasche," *Ann. Phys. Chem. (Poggendorff)*, 91, 56-82, 179-213 (1854).
3. A. Werner, "Quantitative messungen der an- und abklingung getrennter phosphoreszenzbanden," *Annalen der Physik*, 329 (11), 164-190 (1907).
4. T. Förster, "Experimental and theoretical investigation of intermolecular transfer of electron activation energy," *Zeits. Naturforsch.*, 4a, 321 (1949).
5. X. Wang, B. Shapiro, and E. Smela, "Visualizing ion currents in conjugated polymers," *Adv. Mater.*, 16 (18), 1605-1609 (2004).
6. X. Wang, B. Shapiro, and E. Smela, "Ion transport in conjugated polymers: Part 2. Modeling," in preparation (2006).
7. T. F. Otero and J. Padilla, "Anodic shrinking and compaction of polypyrrole blend: electrochemical reduction under conformational relaxation kinetic control," *J. Electroanal. Chem.*, 561, 167-171 (2004).
8. T. F. Otero, H. Grande, and J. Rodriguez, "Conformational relaxation during polypyrrole oxidation: From experiment to theory," *Electrochim. Acta*, 41 (11/12), 1863-1869 (1996).
9. T. F. Otero and I. Boyano, "Comparative study of conducting polymers by the ESCR model," *J. Phys. Chem. B*, 107, 6730-6738 (2003).
10. H. Grande, T. F. Otero, and I. Cantero, "Conformational relaxation in conducting polymers: effect of polymer-solvent interactions," *J. Non-Cryst. Solids*, 235, 619-622 (1998).
11. T. F. Otero, H. Grande, and J. Rodriguez, "Influence of the counterion size on the rate of electrochemical relaxation in polypyrrole," *Synth. Met.*, 83, 205 (1996).
12. H. Grande and T. F. Otero, "Conformational movements explain logarithmic relaxation in conducting polymers," *Electrochim. Acta*, 44, 1893-1900 (1999).
13. T. F. Otero and H. J. Grande, "Reversible 2D to 3D electrode transitions in polypyrrole films," *Colloid Surf. A*, 134 (1-2), 85-94 (1998).
14. T. F. Otero, H. Grande, and J. Rodriguez, "A new model for electrochemical oxidation of polypyrrole under conformational relaxation control," *J. Electroanal. Chem.*, 394, 211 (1995).

15. T. F. Otero and H. Grande, "Thermally enhanced conformational relaxation during electrochemical oxidation of polypyrrole," *Electroanal. Chem.*, 414, 171 (1996).
16. T. F. Otero, M. T. Cortes, and I. Boyano, "Molar enthalpy of the polypyrrole electrochemistry," *J. Electroanal. Chem.*, 562, 161-165 (2004).
17. T. F. Otero and I. Boyano, "Potentiostatic oxidation of polyaniline under conformational relaxation control: Experimental and theoretical study," *J. Phys. Chem. B*, 107, 4269-4276 (2003).